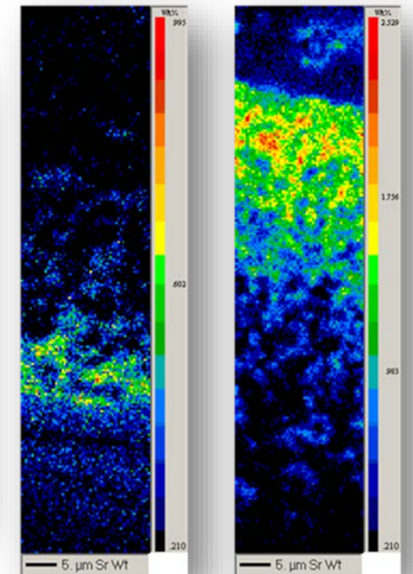
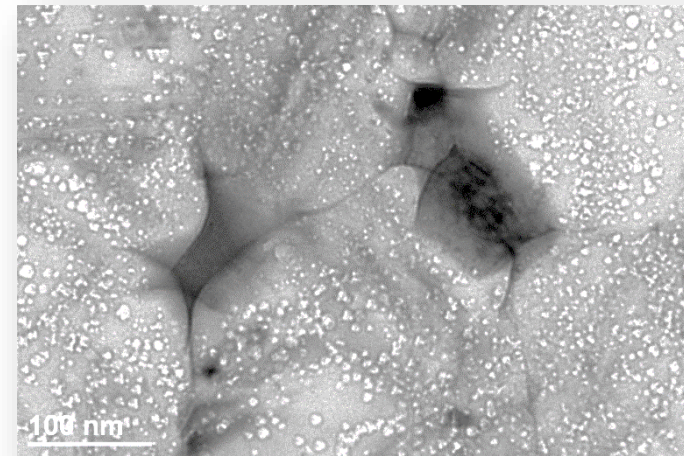


AGR TRISO Fuel Advanced Microscopy and Micro-analysis Results: FY2017 Progress

**AGR TRISO Fuels Program Review
July 18-19, 2017**

**I. J. van Rooyen, T. M. Lillo, K. Wright, S. Meher, M. Cook,
C. Parga, J. Rosales, H Wen**

18 July 2017



INL/MIS-17-42684

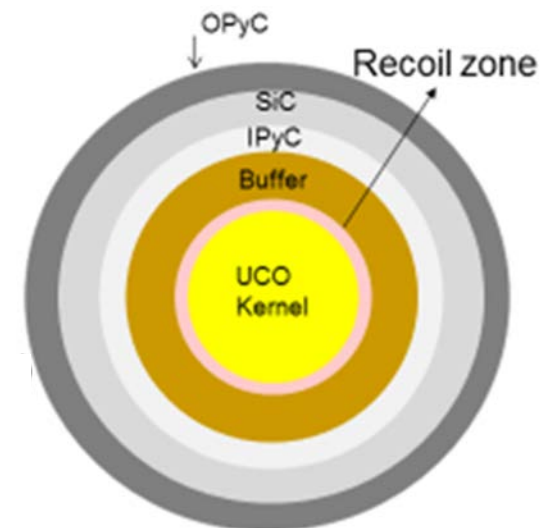
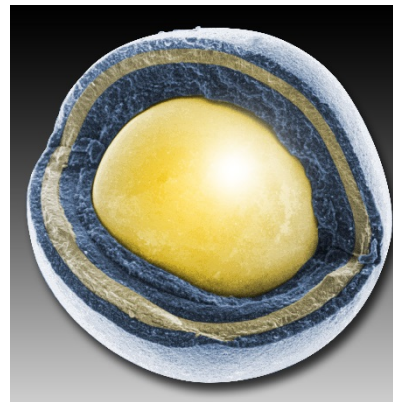
Advanced Gas Reactor Fuels Program Review Meeting, July 18-19, 2017, Idaho Falls, Idaho

www.inl.gov



Outline

- Background and Objectives
- Summary AGR-1 Fission Product Distribution and Identification
- Fission product transport mechanisms
- AGR-2 Advanced Microscopy Preliminary Results (2016 to current)
- Kernel Examination (2016 to current)
- Preliminary Thermodynamic evaluation
- Publications/Reports
- Collaborations
- Conclusions
- Recommendations: Future Work
- Contribution Towards Program Goals
- Acknowledgements

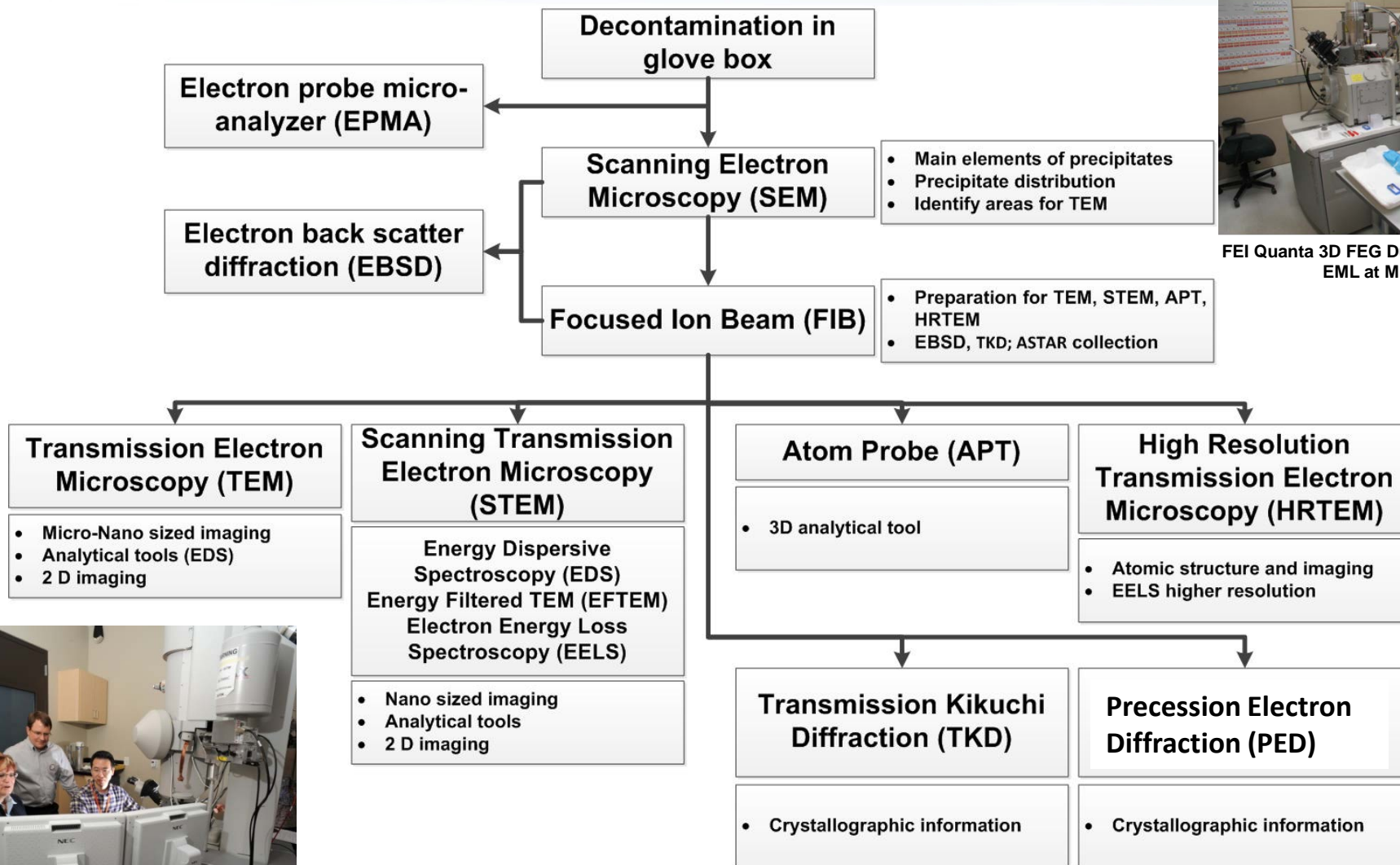


Background: Advanced Microscopy Objectives

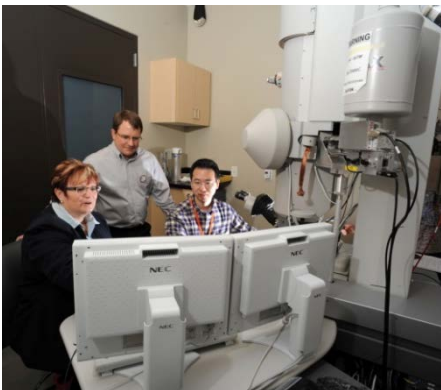
- Characterize effects of radiation upon:
 - kernel porosity
 - layer degradation or corrosion,
 - layer debonding,
 - fission product precipitation,
 - microstructure (layers and fuel)
 - grain characteristics.
- Determine microstructural differences between particles exhibited high and low releases of Ag-110m: understanding transport mechanisms.
- AGR-1 basic electron microscopy, advanced microscopy and micro-analysis: shakedown of methods, procedures and data value proposition (2012-2016)

[van Rooyen I. J., T. Lillo, H. Wen, K. Wright, J. Madden, J. Aguiar, 2017, Advanced Electron Microscopy and Micro analytical technique development and application for Irradiated TRISO Coated Particles from the AGR 1 Experiment, **INL/EXT-15-36281**, January 2017].

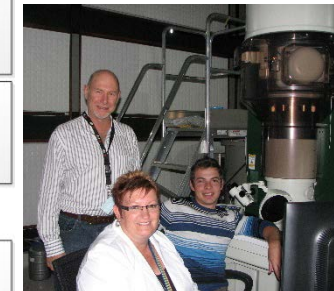
Advanced Microscopy & Micro-analysis Techniques



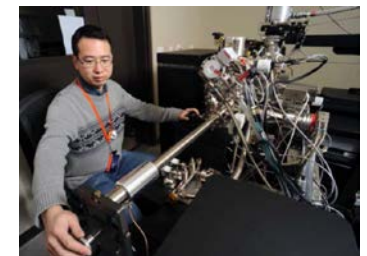
FEI Quanta 3D FEG Dualbeam FIB at EML at MFC



FEI Tecnai G² F30 STEM at the Center for Advanced Energy Studies (CAES)

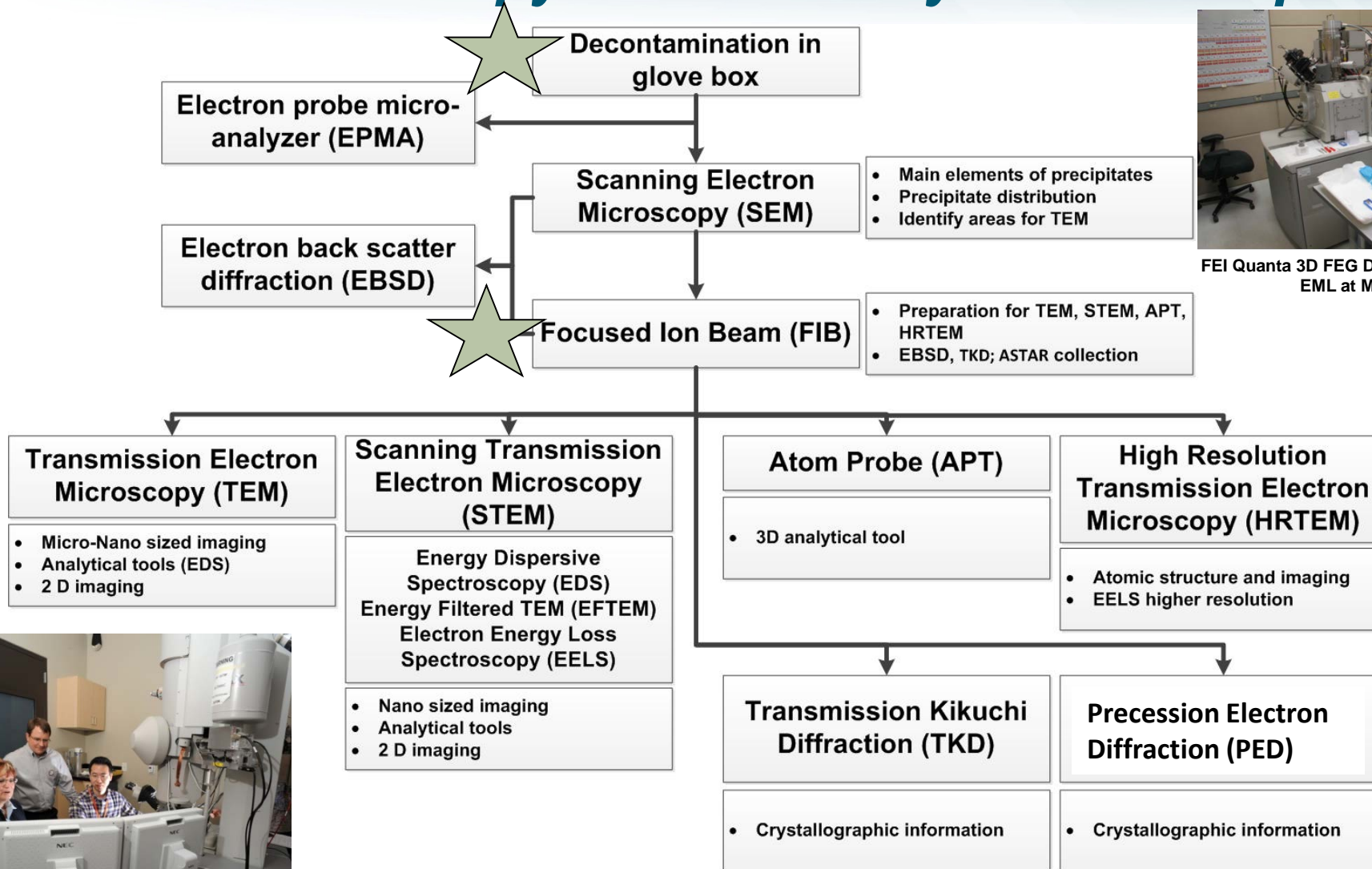


JEOL ARM 200F TEM two CEOS spherical aberration correctors



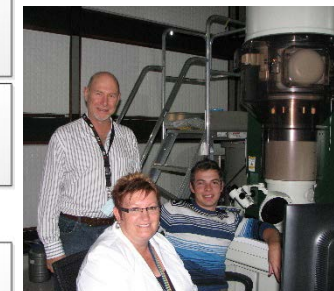
Cameca LEAP 4000XHR at CAES

Advanced Microscopy & Micro-analysis Techniques

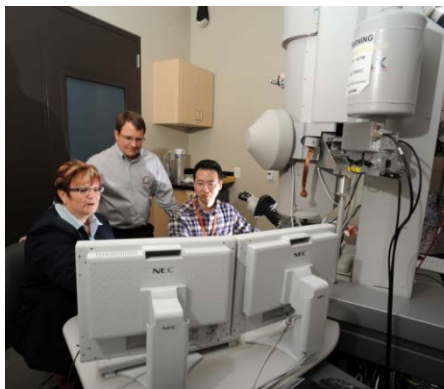


FEI Quanta 3D FEG Dualbeam FIB at EML at MFC

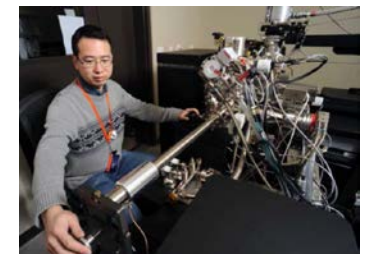
Sample preparation



JEOL ARM 200F TEM two CEOS spherical aberration correctors

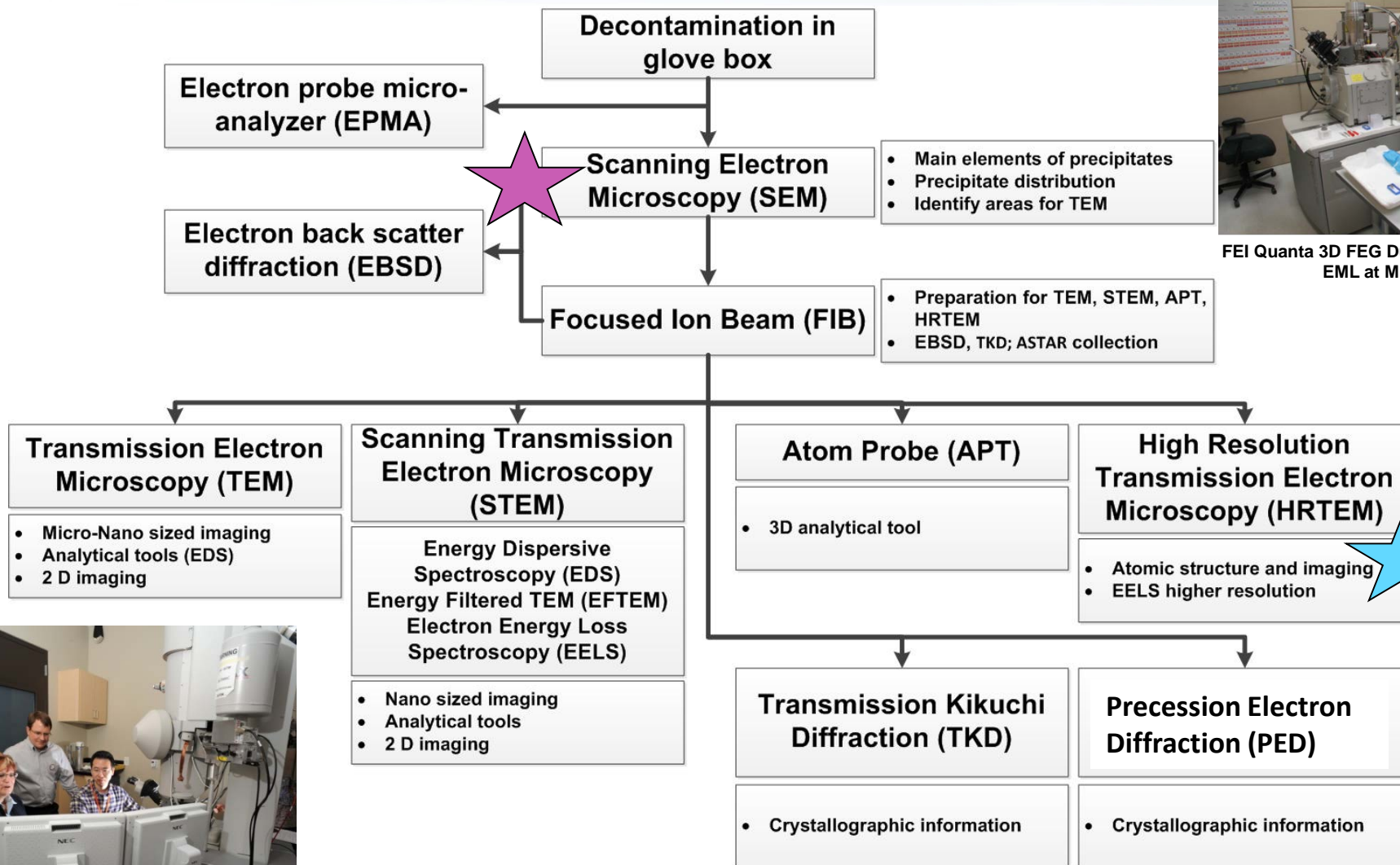


FEI Tecnai G² F30 STEM at the Center for Advanced Energy Studies (CAES)



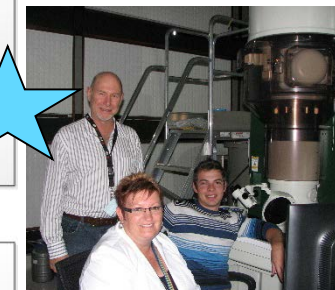
Cemelec LEAP 4000XHR at CAES

Advanced Microscopy & Micro-analysis Techniques

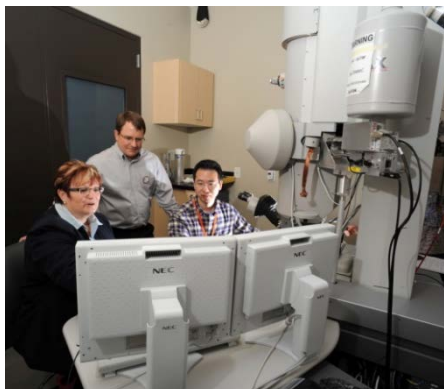


FEI Quanta 3D FEG Dualbeam FIB at EML at MFC

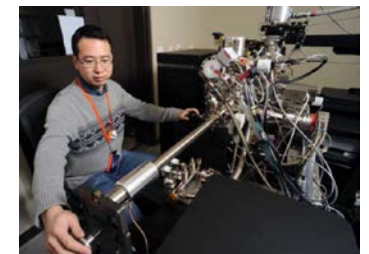
Layer Degradation/Corrosion
 Layer Debonding
 Fission Product Clusters
 Fission Product Mapping



JEOL ARM 200F TEM two CEOS spherical aberration correctors

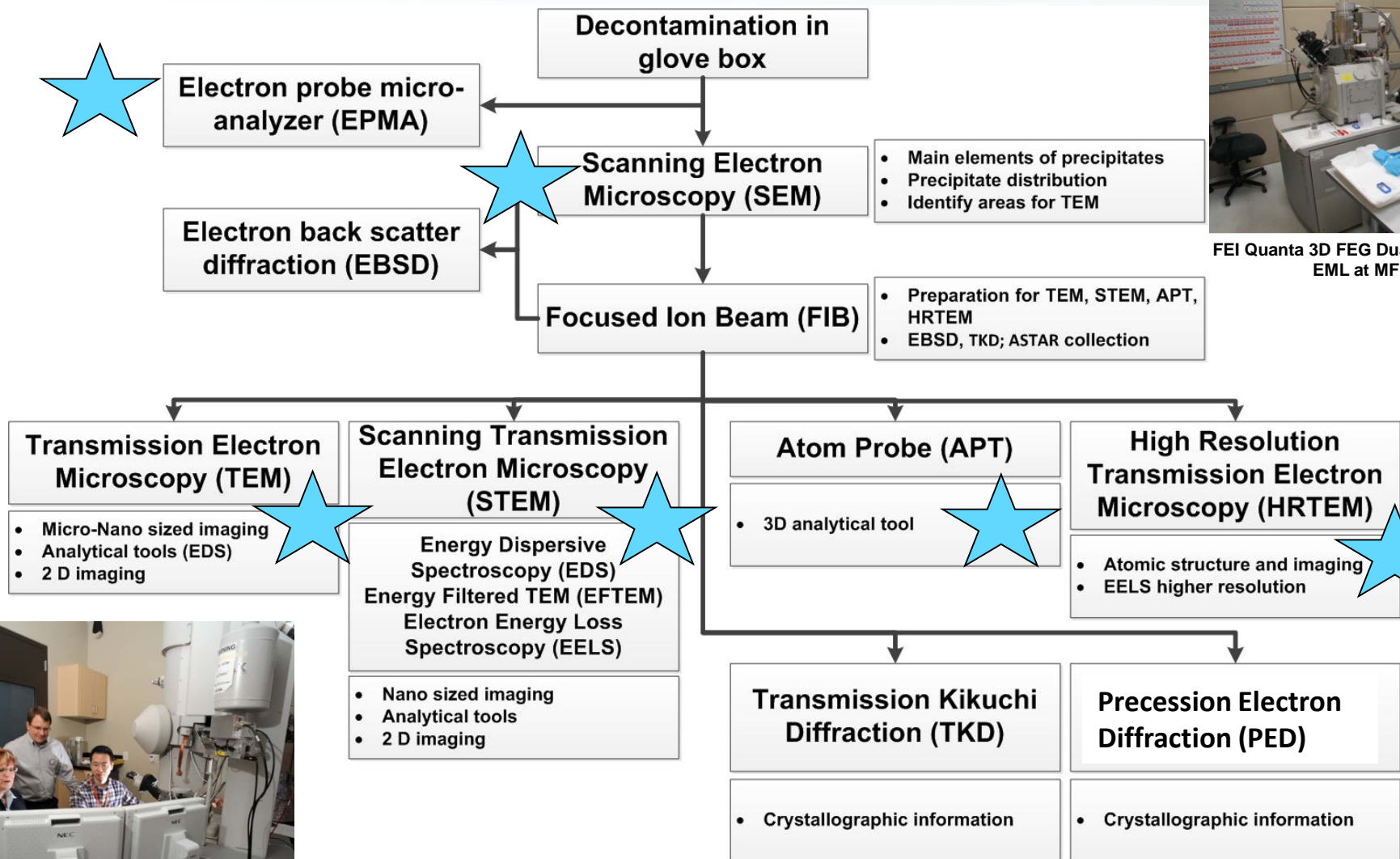


FEI Tecnai G² F30 STEM at the Center for Advanced Energy Studies (CAES)



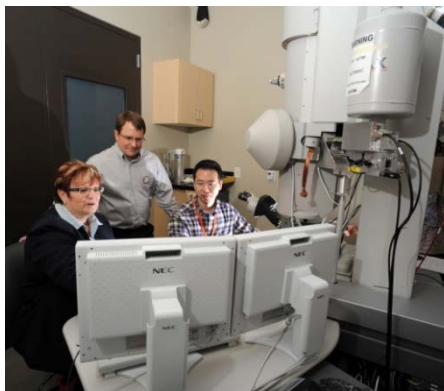
Cameca LEAP 4000XHR at CAES

Advanced Microscopy & Micro-analysis Techniques

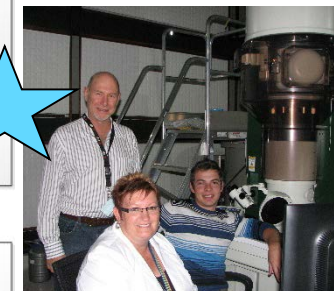


FEI Quanta 3D FEG Dualbeam FIB at EML at MFC

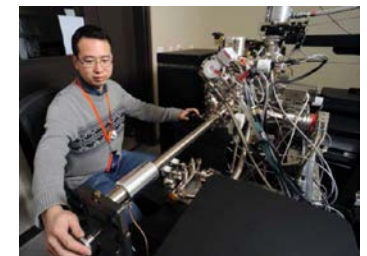
FISSION PRODUCT IDENTIFICATION AND LOCATION



FEI Tecnai G² F30 STEM at the Center for Advanced Energy Studies (CAES)

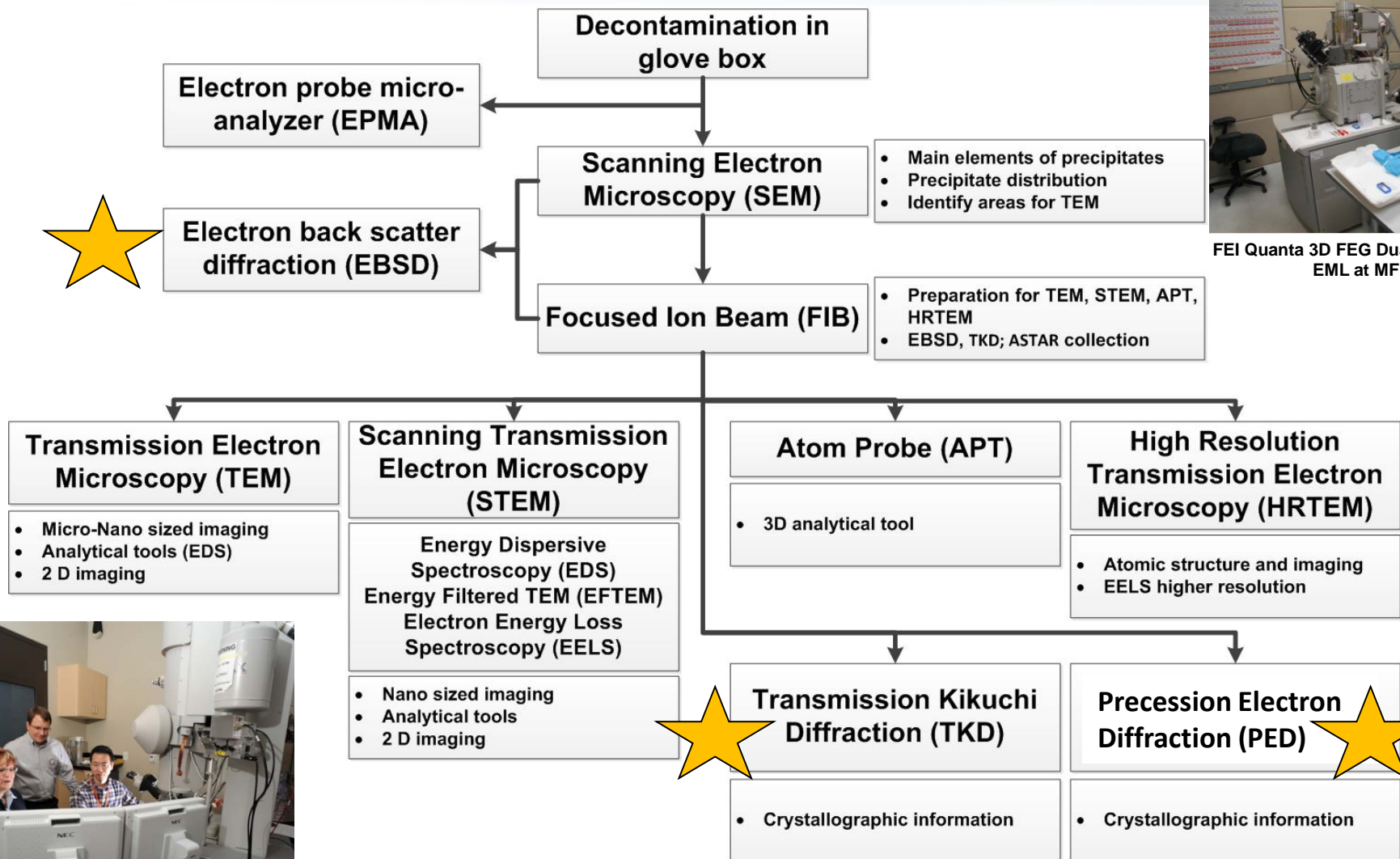


JEOL ARM 200F TEM two CEOS spherical aberration correctors



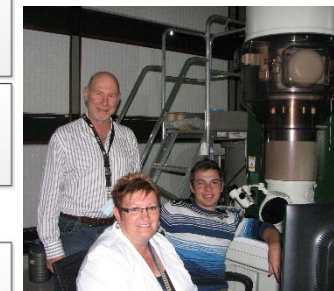
Cameca LEAP 4000XHR at CAES

Advanced Microscopy & Micro-analysis Techniques

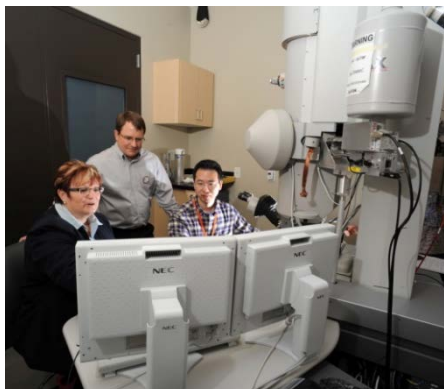


FEI Quanta 3D FEG Dualbeam FIB at EML at MFC

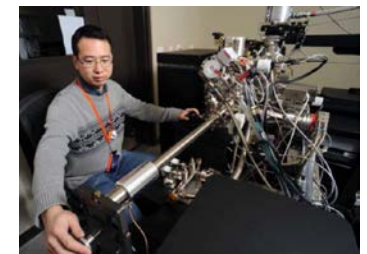
GRAIN BOUNDARY CHARACTERISTICS



JEOL ARM 200F TEM two CEOS spherical aberration correctors

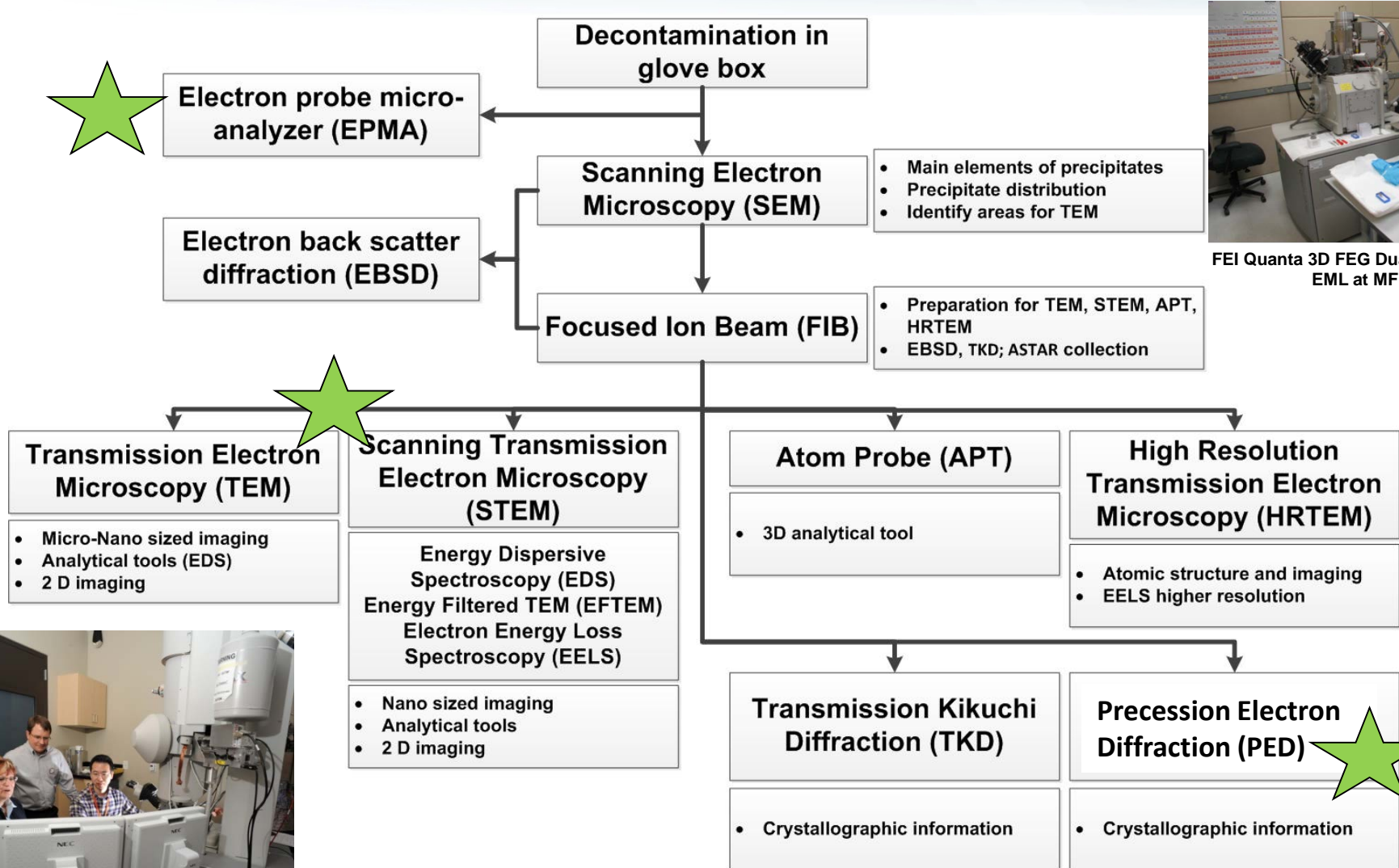


FEI Tecnai G² F30 STEM at the Center for Advanced Energy Studies (CAES)



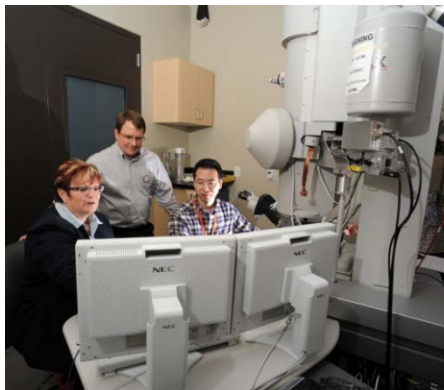
Cameca LEAP 4000XHR at CAES

Advanced Microscopy & Micro-analysis Techniques

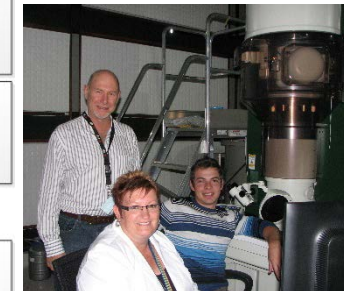


FEI Quanta 3D FEG Dualbeam FIB at EML at MFC

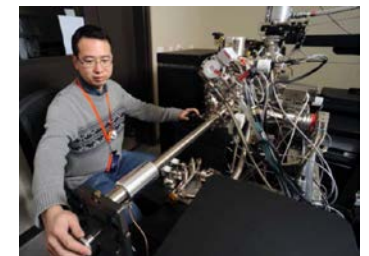
Preferred Methods after AGR-1 Shakedown



FEI Tecnai G² F30 STEM at the Center for Advanced Energy Studies (CAES)

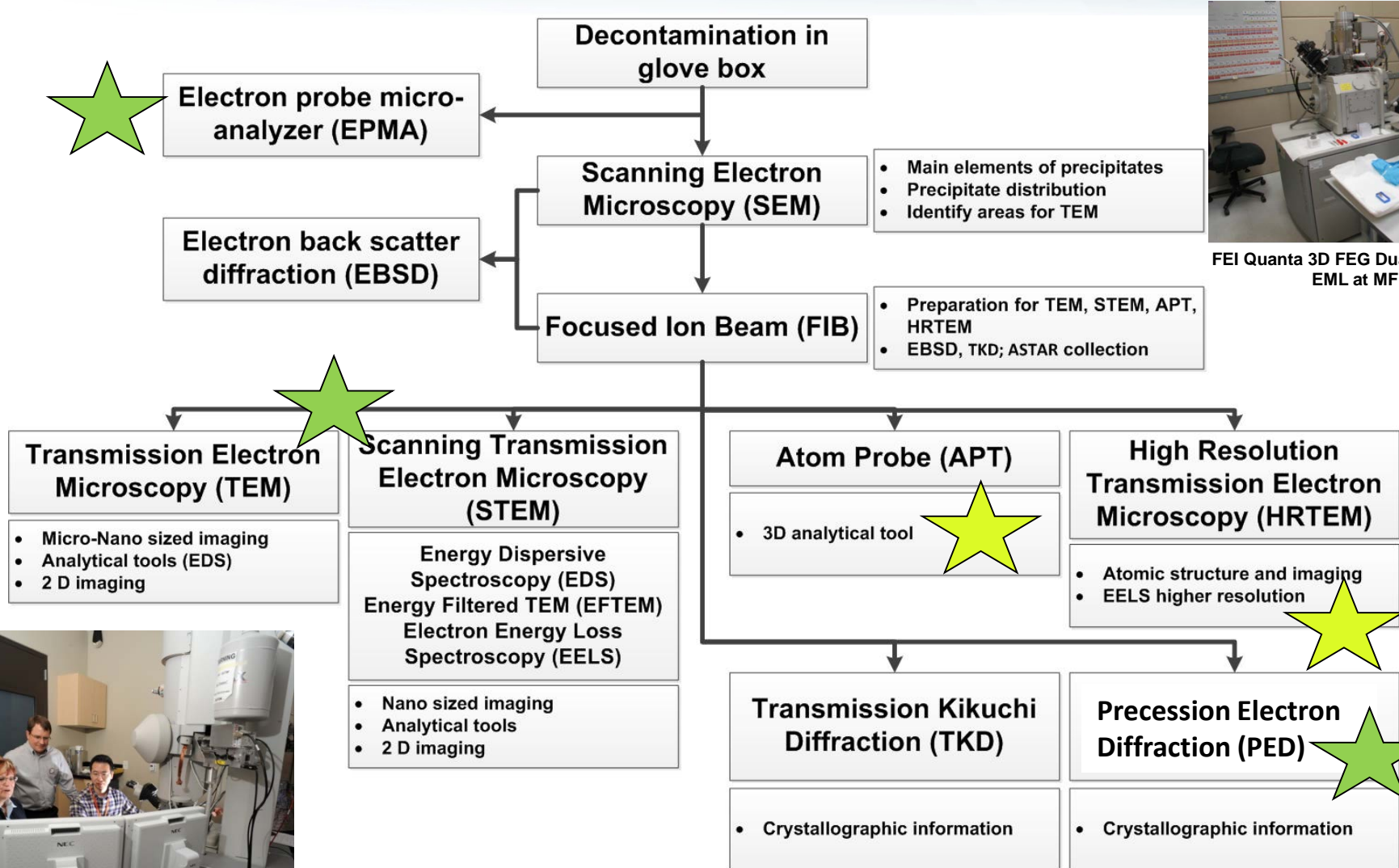


JEOL ARM 200F TEM two CEOS spherical aberration correctors



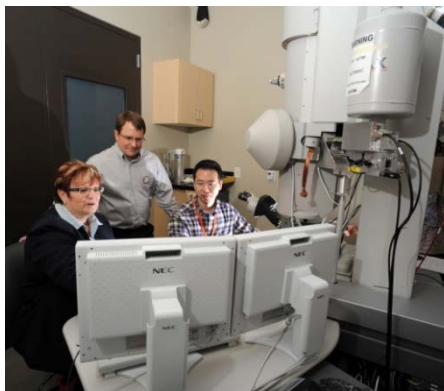
Cameca LEAP 4000XHR at CAES

Advanced Microscopy & Micro-analysis Techniques

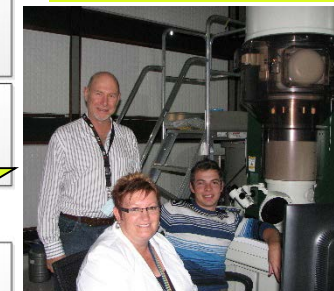


FEI Quanta 3D FEG Dualbeam FIB at EML at MFC

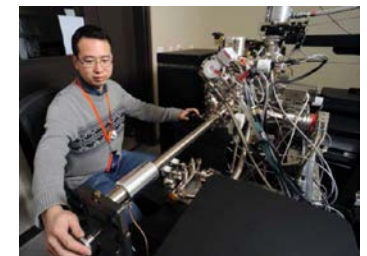
Preferred Methods after AGR-1 Shakedown
Specialized Applications



FEI Tecnai G² F30 STEM at the Center for Advanced Energy Studies (CAES)



JEOL ARM 200F TEM two CEOS spherical aberration correctors



Cameca LEAP 4000XHR at CAES

Significant AGR-1 Technical Findings: Particle History

Compact	Fuel Type	Burnup (%FIMA)	Fast Neutron Fluence	Time-Average Volume Average Temp. (°C)	Time-Average Peak Temp. (°C)	Particles studied
6-3-2	Baseline	11.4	2.55	1070	1144	AGR1-632-030 (Low Ag (21%) retention) AGR1-632-034 (High Ag (65 %) retention) AGR1-632-035 (High (79%) Ag retention)
5-3-1	Variant 1	16.7	3.60	1040	1122	AGR1-531-038 (Low (< 19%) Ag retention) AGR1-531-031 (High (105%) Ag retention)
5-2-3	Variant 1	17.4	3.77	1059	1141	AGR-523-SP01 (16% Ag retention)
1-3-1	Variant 3	15.3	3.22	1092	1166	AGR1-131-099 (Low (<6 %) Ag retention) AGR1-131-066 (High (39%) Ag retention)
4-1-1	Variant 3	19.4	4.13	1072	1182	AGR1-411-030 (High Ag (90%) retention)
4-3-3	Variant 3	18.6	4.16	1094	1179	AGR1-433-003 (Low (< 22%) Ag retention) AGR1-433-007 (High (100%) Ag retention) AGR1-433-001 (Low (66%) Ag retention) AGR1-433-004 (High (99%) Ag retention)

Fuel Type	IPyC temp. (°C)	IPyC coating gas fraction	SiC temp. (°C)
Baseline	1265	0.30	1500
Fabricated to closely match historically proven German fuel containing UO ₂ kernels.			
Variant 1	1290	0.30	1500
Enhanced irradiation stability of the pyrocarbon (PyC), although permeability expected to increase and, consequently, uranium dispersion (IPyC layer less dense than that in baseline fuel) by changing IPyC deposition temperature.			
Variant 3^a	1265	0.30	1425
^a Reduce the potential for SiC-layer defects resulting from uranium dispersion and provide a change in polycrystalline microstructure that may be less permeable to metallic fission			

[J. D. HUNN, G. E. JELLISON, JR., and R. A. LOWDEN, "Increase in Pyrolytic Carbon Optical Anisotropy and Density During Processing of Coated Particle Fuel Due to Heat Treatment," *J. Nucl. Mater.*, **374**, 445 (2008).]

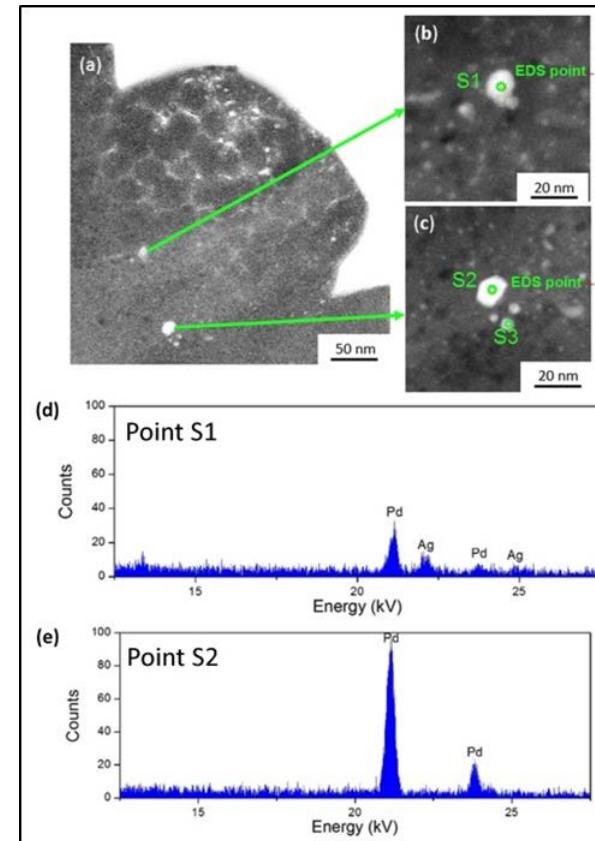
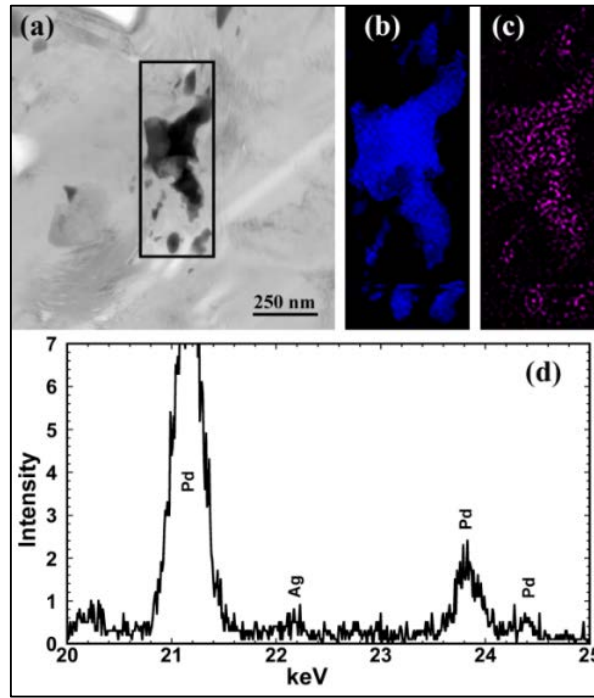
[P. A. DEMKOWICZ, J. D. HUNN, R. N. MORRIS, I. VAN ROOYEN, T. GERCZAK, J. M. HARP, and S. A. PLOGER, "AGR-1 Post Irradiation, Examination Final Report," Idaho National Laboratory INL/EXT-15-36407 (2015).]

[I.J. van Rooyen, T.M. Lillo, H. Wen, K.E. Wright, J. Madden, J. Aguiar, Advanced Electron Microscopy and Micro Analytical Technique Development and Application on Irradiated TRISO Coated Particles from the AGR-1 Experiment, INL/EXT-15-36281, January 2017]

Conclusions from AGR-1 Advanced Microscopy

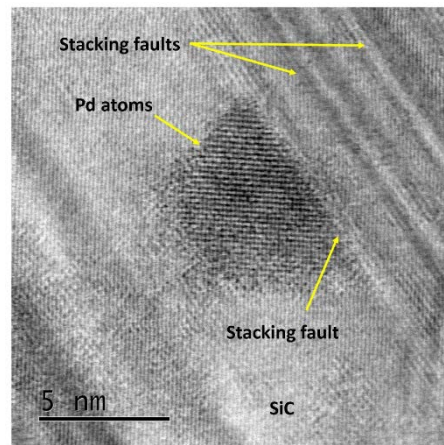
- The deployment and adaption of advanced nano-scaled techniques set a benchmark for future studies.
- Ag is identified at both intra- and inter-granular sites within the SiC microstructure, although it is predominantly in grain boundaries and triple points.

Co-existence of Pd (38.5 at.%) and Ag 4.4 at.%)

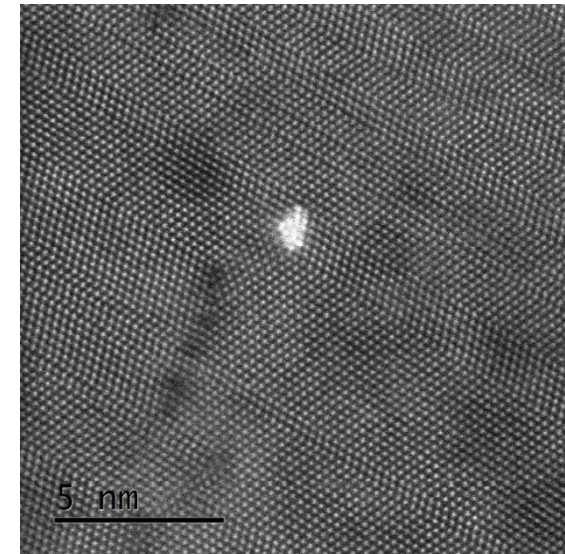
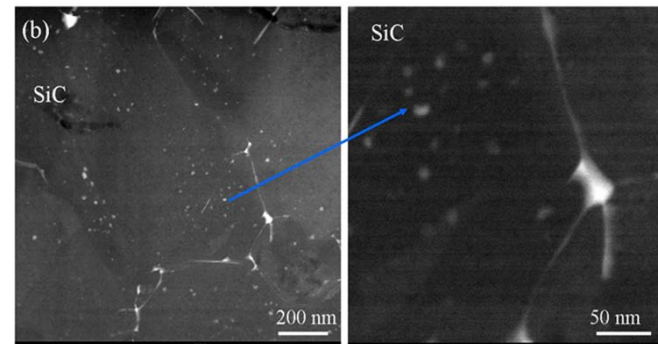


Conclusions from AGR-1 Advanced Microscopy

- Pd dominated most of the fission product precipitates examined:
 - found throughout the SiC layer thickness, either separately or co-existing, with other elements.
 - Intra- or intergranular locations
- U both intra- or intergranular locations



[Van Rooyen, I. J., E. J. Olivier and J. H. Neethling, "Investigation of the Fission Products Silver, Palladium and Cadmium in Neutron Irradiated SiC using a Cs Corrected HRTEM", Journal of Nuclear Materials, 476 (2016) 93 – 101]



[E. J. Olivier, J. H. Neethling, IJ van Rooyen "Cs-corrected STEM and EDS Investigation of Pd and Ag Transport Along SiC Grain Boundaries and Dislocations, 4th SiC workshop, Batou, China, June 2017]

- Precipitates can be single- and multi-phased as determined by chemical composition
- Initial HRTEM studies showed that Pd-rich nano precipitates have a cubic structure in grain boundaries and triple points

Precipitate Element Combination Summary

Particle	Precipitate Element Combinations in the SiC Layer		
	Inner Area	Center Area	Outer Area
AGR1-632-035 (High (79%) Ag retention)	Pd, Ag	Pd, Ag, Ce	Pd
	Pd-Ag, Pd-Pu, Pd-U, Pd-Ce	Pd-Ag, Pd-U, Pd-Ce,	Pd-Ag, Pd-Eu, Pd-Ce
	Pd-Ag-Cd, Pd-U-Pu, Pd-Ag-Cs-U		Pd-Ag-Ce, Pd-Ce-Eu
AGR1-531 - 038 (Low (< 19%) Ag retention)	Pd	Pd, Ag	Pd
	Pd-U, Pd-Pu, Pd-Ag	Pd-Ag, Pd-Pu, Pd-U, Pd-Ce	
	Pd-Cs-Eu, Pd-Ce-Eu, Pd-Cs-Ag, Pd-U-Pu, Pd-Ag-Eu	Pd-Ag-U, Pd-U-Pu, Pd-Ag-Pu	Pd-U-Pu
AGR1-531 - 031 (High (105%) Ag retention)	Pd, Cs, Pu, U, Ce, Ag-U, Cs-U, Ce-U, U-Pu		
AGR1-131-066 (High (39%) Ag retention)	Pd, U	Pd	Pd
	Pd-Si, U-Si, Pd-U, Cs-U	Pd-Si, Pd-U	Pd-U, Pd-Ce
	Pd-Si-U	Pd-Si-U	Pd-Ce-U
AGR1-131-099 (Low (<6%) Ag retention)	Pd, U	Pd	Pd
	Pd-U, U-Cs, Pd-U	Pd-U	Pd-U
	Pd-U-Ce, Pd-U-Cs Pd-U-Cs-Ce		
AGR1-433-001 (Low (66%) Ag retention)	Ag, Pd	Pd	Pd
	Ag-Cs, Pd-Ce, Pd-Ag, Pd-U, Ce-U, Pd-Pu	Pd-U,	Pd-Ag, Pd-Eu, Pd-Ce
	Pd-Ag-Ce, Pd-Ce-U, Pd-Ce-Pu, Pd-U-Pu, Pd-Ag-U	Pd-Ce-Eu, Pd-Cs-Pu, Pd-Ce-U	Pd-Eu-U
	Pd-Ce-U-Pu, Pd-Eu-U-Pu, Pd-Ce-Eu-U, Pd-U-Pu-Ce	Pd-Ce-Eu-Pu, Pd-Ag-Ce-Eu	Pd-Ag-Cs-Eu-U
		Pd-Ag-Cs-Eu-U Pd-Ag-Ce-Eu-U-Pu	
AGR1-433-004 (High (98%) Ag retention)	Pd, Ag	Pd	Pd
	Pd-U, Pd-Ce, Pd-Ag, Pd-Eu	Pd-Ce	Pd-Ag
	Pd-Ce-Pu, Pd-U-Pu, Pd-Ag-Ce		Pd-Cs-Eu

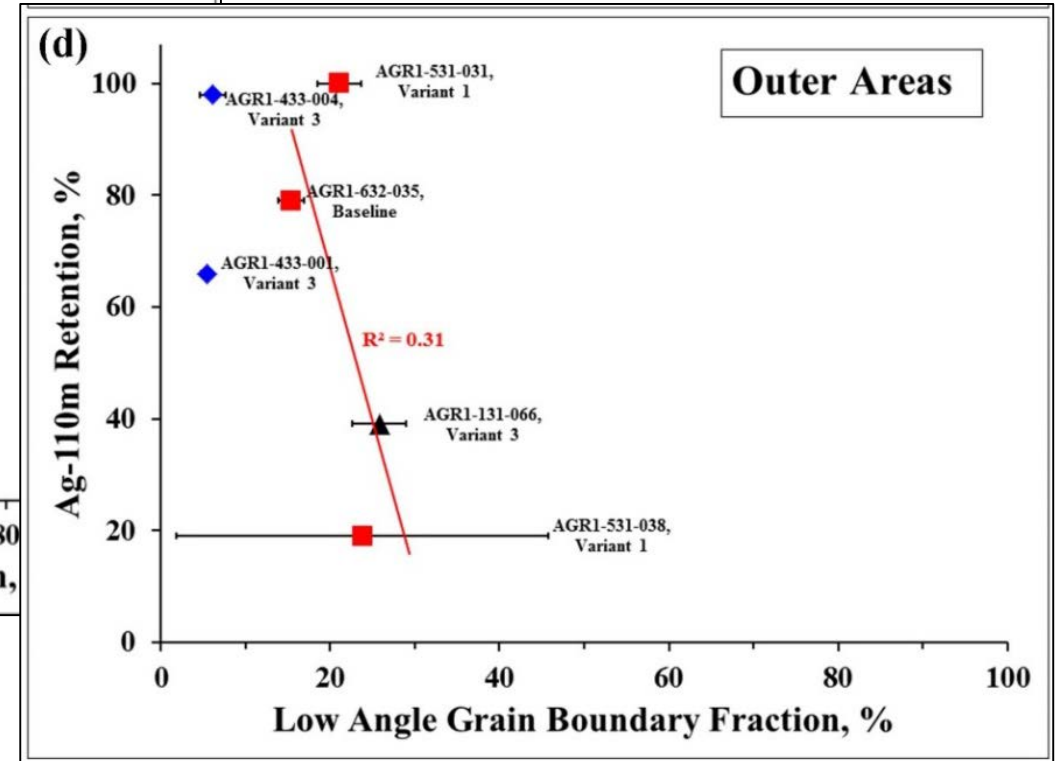
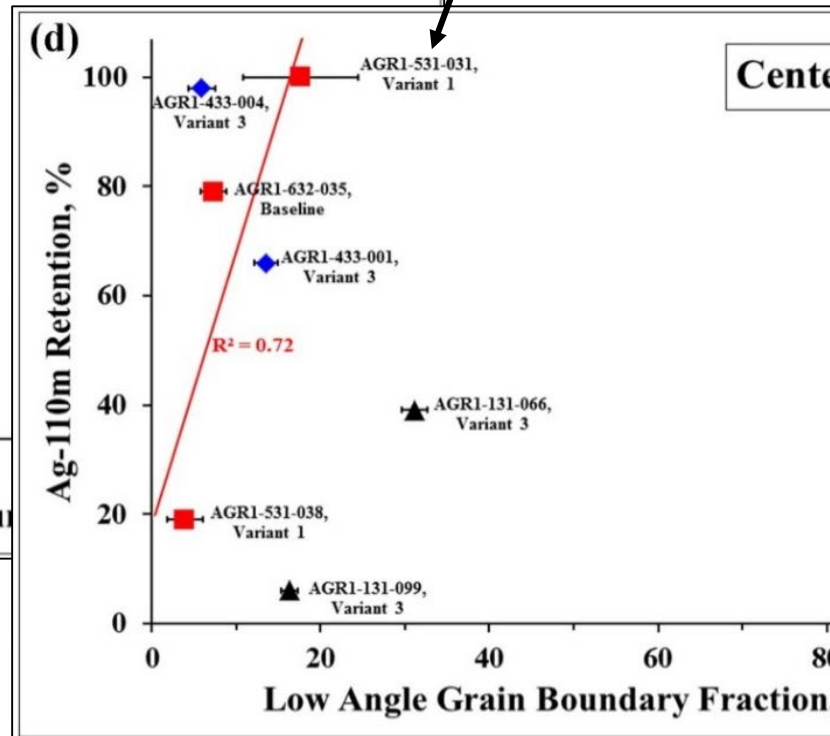
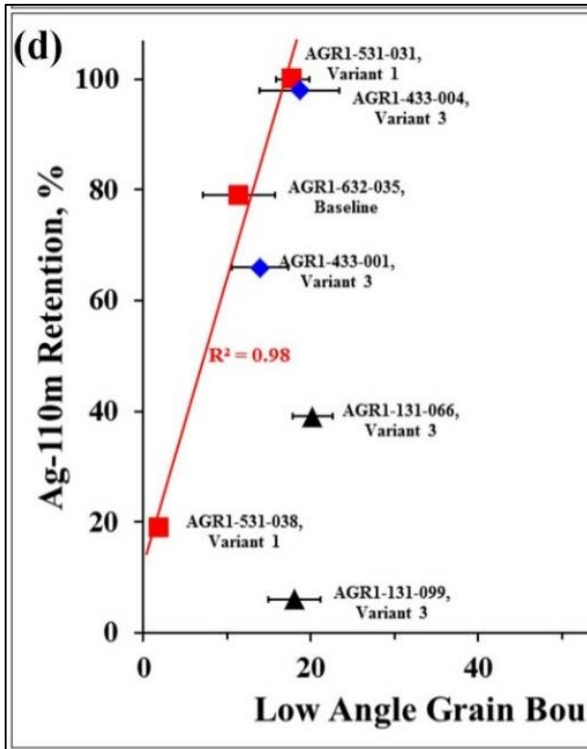
Precipitate Element Combination Summary

Particle	Precipitate Element Combinations in the SiC Layer		
	Inner Area	Center Area	Outer Area
<p>Combinations of elements in more than 700 precipitates that were examined:</p> <ul style="list-style-type: none"> – Complex and varying in nature – More element combinations exist for precipitates from particles with relatively low Ag retention compared to particles with relatively high Ag-retention irrespective of fuel type. – Cs present in particles from all compacts evaluated. – Often other elements (e.g., Eu, Ce, Pu, and Cs) can be present in precipitates that predominantly contain Pd, Si, Ag, and U. – U is predominantly found in combination with other elements and is only found alone in precipitates from Compact 1-3-1, which is a Variant 3 fuel compact. – U and Ag are only found as a combination in the low Ag retention safety-tested particle AGR1-433-001. 			
AGR1-433-004 (High (98%) Ag retention)	Pd, Ag	Pd	Pd
	Pd-U, Pd-Ce, Pd-Ag, Pd-Eu	Pd-Ce	Pd-Ag
	Pd-Ce-Pu, Pd-U-Pu, Pd-Ag-Ce		Pd-Cs-Eu

AGR-1 Grain Boundary Characteristics: Low Angle Boundary

Good + correlation between Ag-110m retention and low-angle grain boundary fraction.

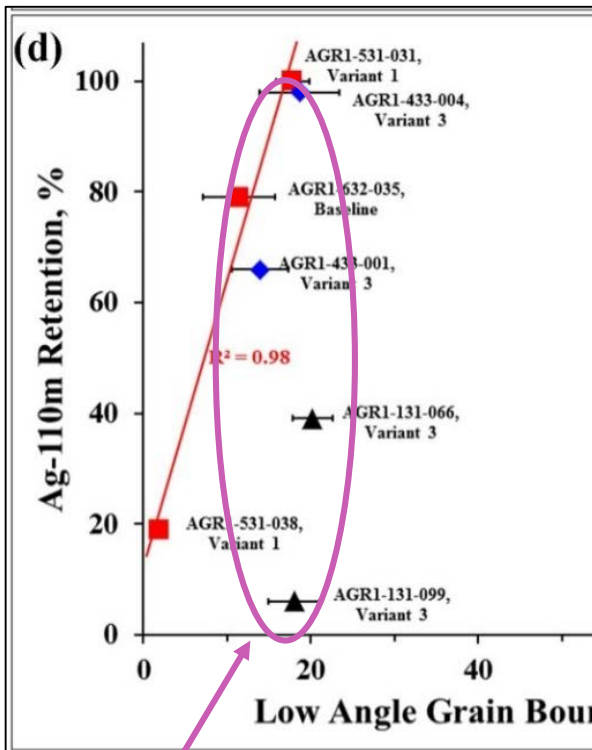
EXPECT
> low angle boundaries = aid Ag retention



Combining datasets from inner, center, and outer regions: weaken correlations between Ag-110m and various grain boundary parameters.

- Relook at increments chosen to determine if groupings consistent and relevant

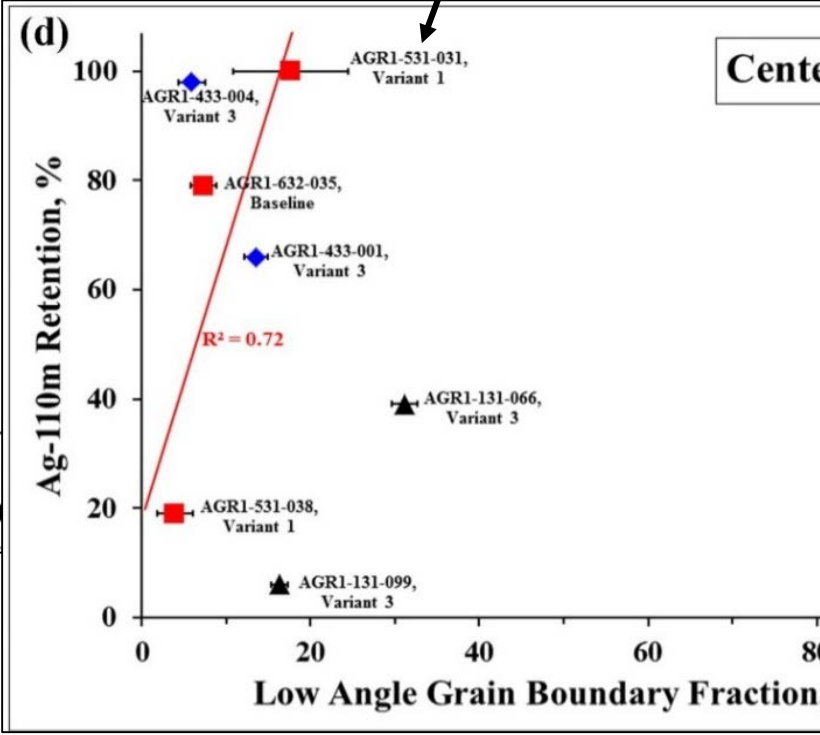
AGR-1 Grain Boundary Characteristics: Low Angle Boundary



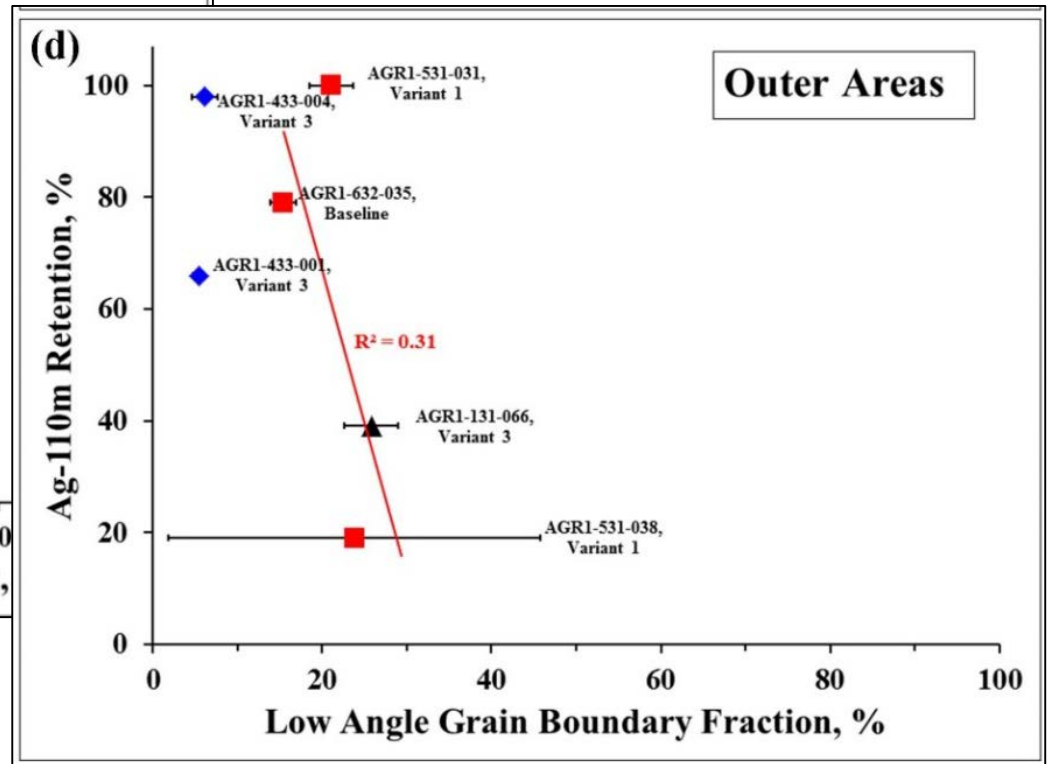
Inner Areas

Good + correlation between Ag-110m retention and low-angle grain boundary fraction.

EXPECT
> low angle boundaries = aid Ag retention



Center Areas



Outer Areas

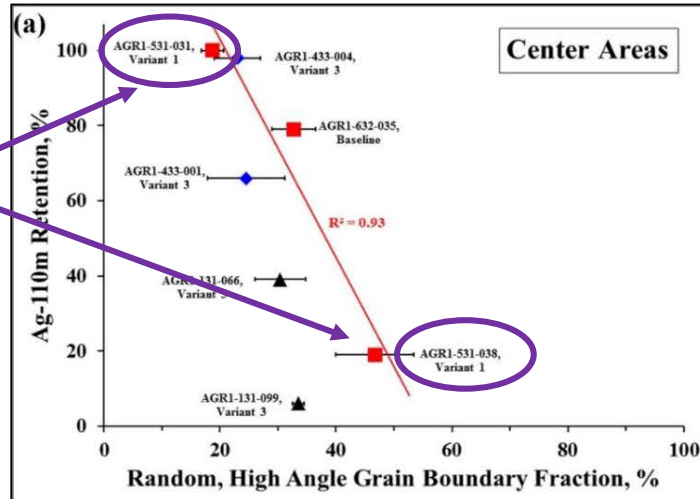
Variant 3 particles: narrow band ~ 20% low angle boundaries

Combining datasets from inner, center, and outer regions: weaken correlations between Ag-110m and various grain boundary parameters.

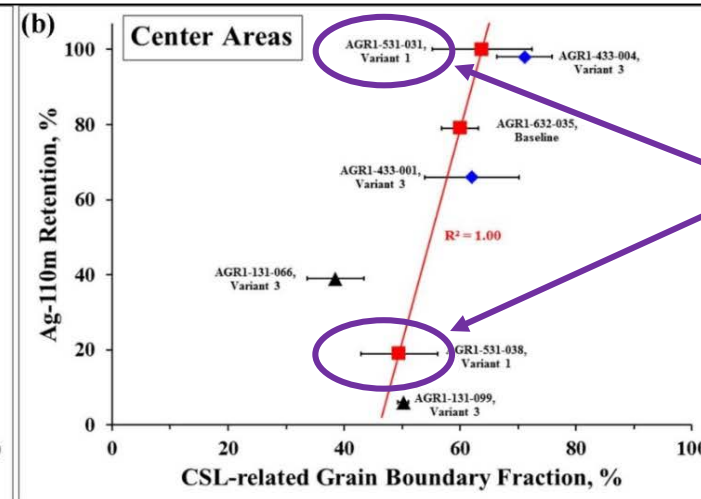
- Relook at increments chosen to determine if groupings consistent and relevant

AGR-1 Grain Boundary Characteristics: Center Area Closer Look

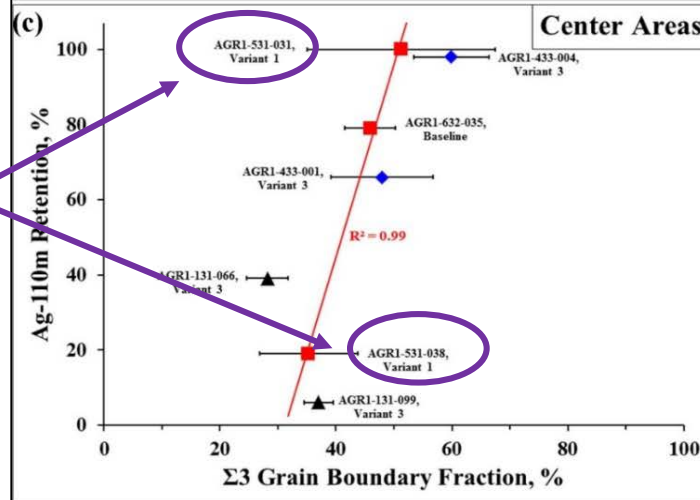
- Correlation Variant 1 Fuel type



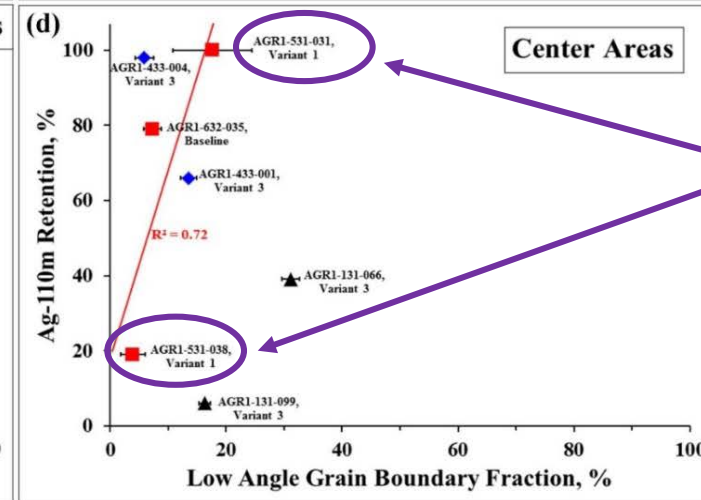
+ Correlation Variant 1 Fuel type



+ Correlation Variant 1 Fuel type

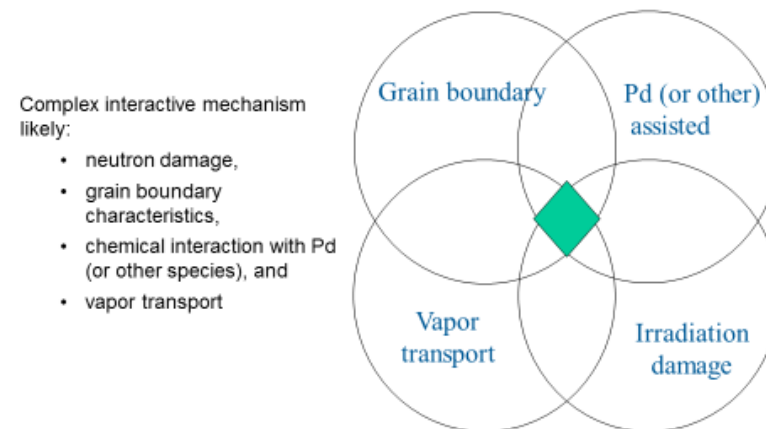


+ Correlation Variant 1 Fuel type



AGR-1 Conclusions (cont.): Fission Product Transport Mechanisms

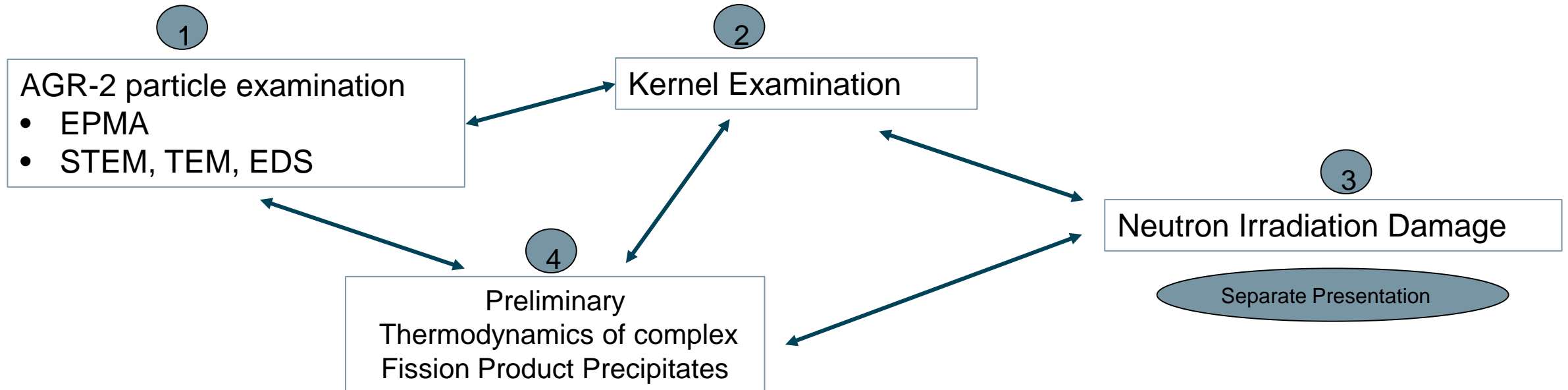
- Although this work was not predominantly focused on fission product mechanistic studies, results and observations contributed toward knowledge on transport mechanisms.
 - No single mechanism hypothesis can be reported.
 - Complexity of mechanisms is further highlighted by the multiple variations of elemental combinations found in the fission product precipitates.
 - Not necessarily true that a chemical-assisted transport mechanism is dominant.
 - Presence of Ag predominantly on grain boundaries suggests that grain boundary transport mechanism may be prominent.
 - Neutron damage and its effects on fission-product transport needs to be considered in future work



[I. J. van Rooyen, H. Nabielek, J. H. Neethling, M. Kania and D.A. Petti, PROGRESS IN SOLVING THE ELUSIVE AG TRANSPORT MECHANISM IN TRISO COATED PARTICLES: "WHAT IS NEW?" Paper 31261, Proceedings of the 2014 International HTR-2014 Conference of High Temperature Reactors, Weihai, China, 2014]

[I.J. van Rooyen, T.M. Lillo, H. Wen, K.E. Wright, J. Madden, J. Aguiar, Advanced Electron Microscopy and Micro Analytical Technique Development and Application on Irradiated TRISO Coated Particles from the AGR-1 Experiment, INL/EXT-15-36281, January 2017]

AGR-2 Advanced Microscopy Preliminary Results (2016 to current)



FY2017 AGR-2 Test Matrix and Scope 1

FIB Research Plan: Particle AGR2-222-RS36 (Mount D25)
 Irradiation History: non detectable Ag, M/C Eu-154: 0.8

Note: Lamellae schematic not to size

SiC lamellae:

1, 2, 3 (inner, center and outer) at Area A A

4, 5, 6 (inner, center and outer) at Area B B

Buffer, PyC lamellae:

7, 8 lamellae through the cluster of precipitates at Area A

9 lamella in IPyC (parallel to the IPyC/IPyC interface) need to contain the bright aligned precipitates in Area B

10 lamella in buffer -IPyC interface parallel to lamella 9 in Area B

Rev 0, 9 January 2017
Isabella van Rooyen

All data collection completed, analysis and interpretation in progress

Note there is 2 particles in this mount, choose the correct one

FIB Research Plan: Particle AGR2-223-RS06 (Mount D07)
 (Irradiation history: M/C = 0.08, 10.8% FIMA; 1261°C TAVA, 2.99 n/m² fast fluence)

Kernel lamellae:

1 center, 2 kernel-buffer interface, 3 Recoil zone -kernel Interface

SiC lamellae:

4, 5, 6 (inner, center and outer) at Area A A

7, 8, 9 (inner, center and outer) at Area B B

10 lamella through the cluster of precipitates

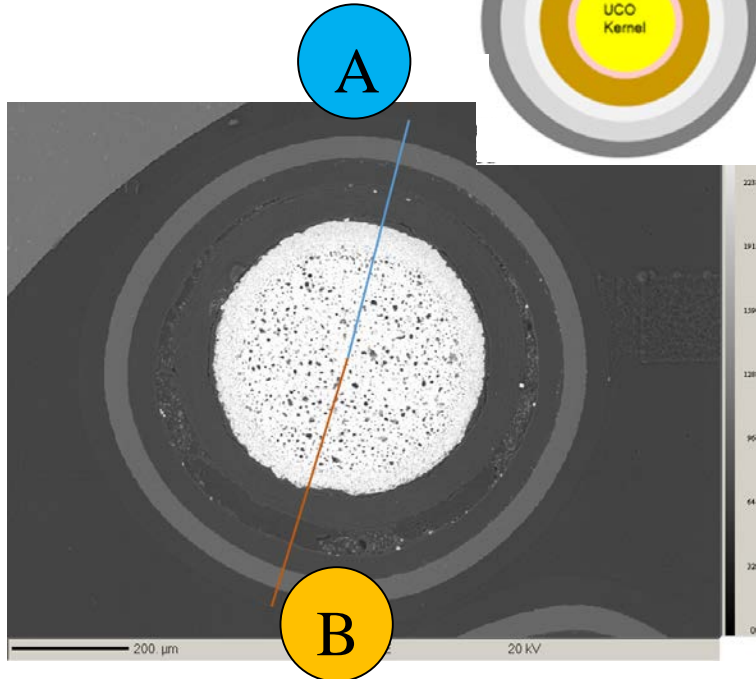
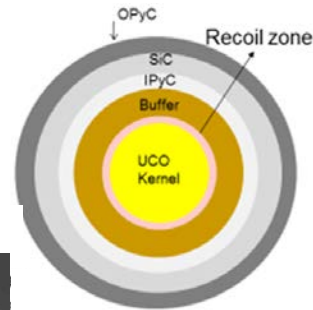
Note: Lamellae schematic not to size

Isabella van Rooyen, 7 July 2016 REV 1

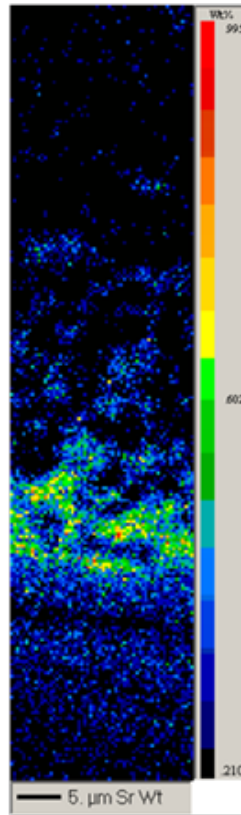
Lamellae prepared, awaiting shipment, microscopy scheduled August/September 2017

EPMA Results

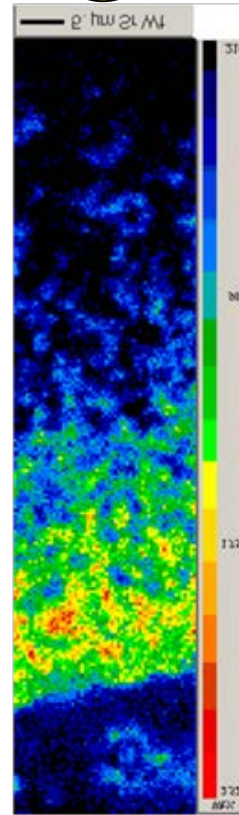
Parameter	Value
²³⁵ U enrichment	14.029
% FIMA average burnup	10.8
Time-average, volume average temperature, °C	1261
Approximate fast fluence ($\times 10^{25}$), n/m ²	3.0
Measured to calculated ^{110m} Ag ratio	0.08



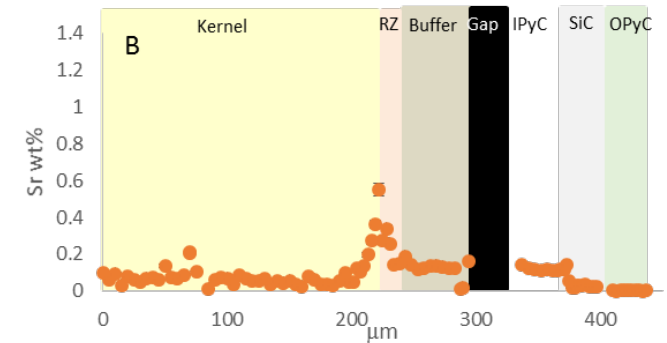
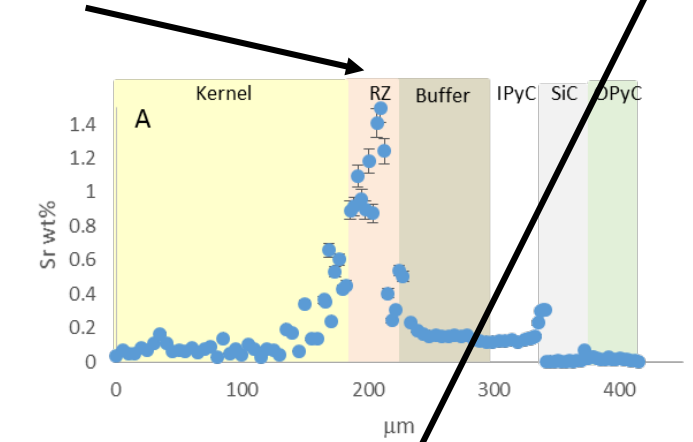
A



B

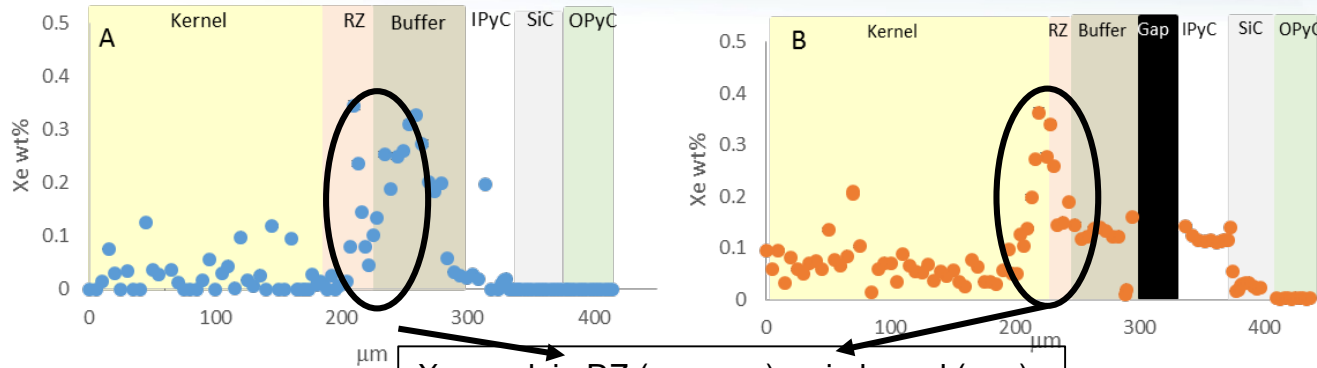


[Sr] in Recoil Zone : non gap side
 (A) 4X higher than gap side (B)

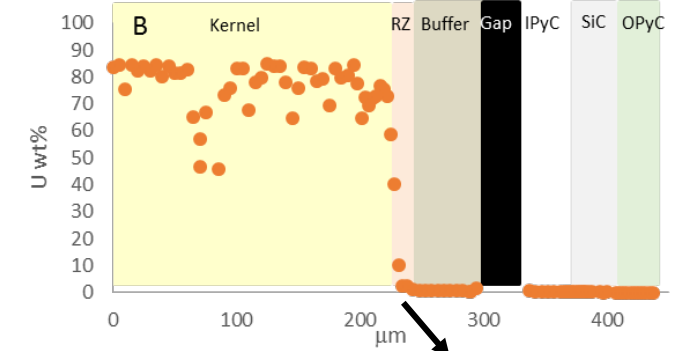
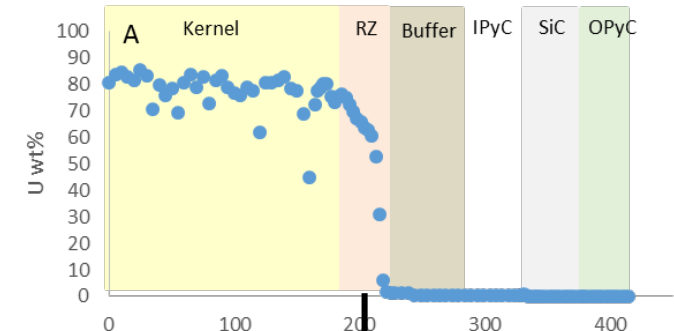
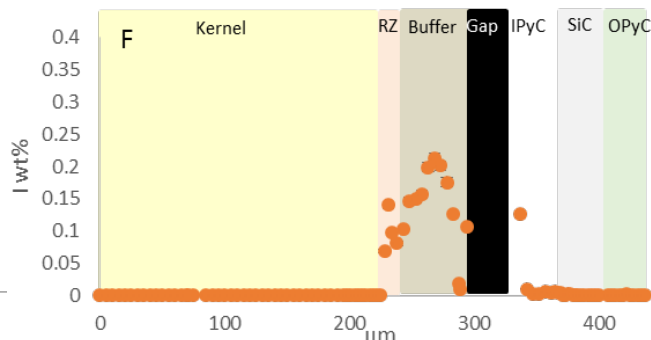
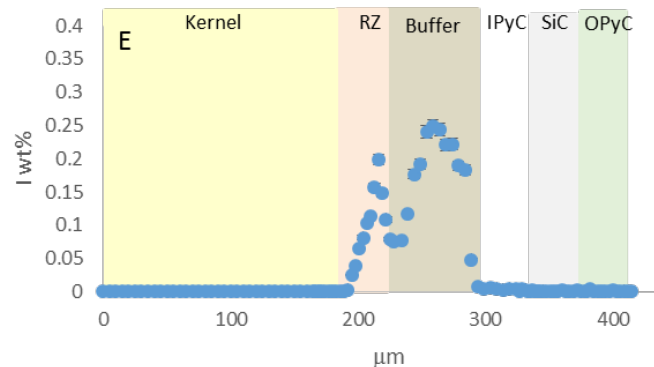
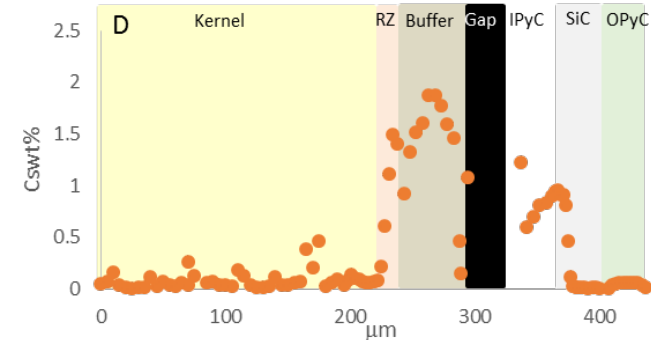
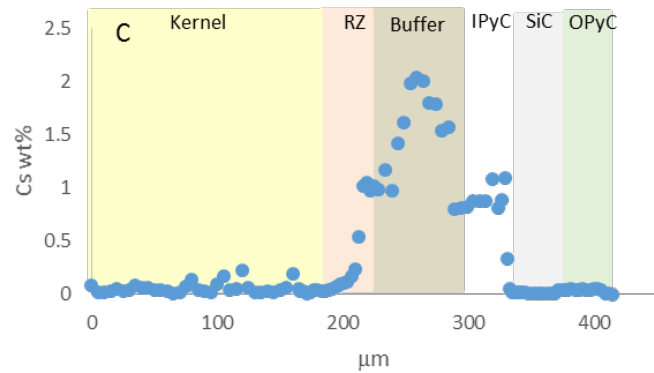


Te, Eu, Sn Similar Behavior

Different behavior: Non-Gap(A: blue) vs Gap (B: orange)



Xe: peak in RZ (non-gap) vs in kernel (gap)



U

- RZ thickness differences

Cs and I similar behavior:

- Highest concentration in buffer
- No significant differences between A and B

La, Ce, Nd, Pr, Sm

- No significant differences between A and B

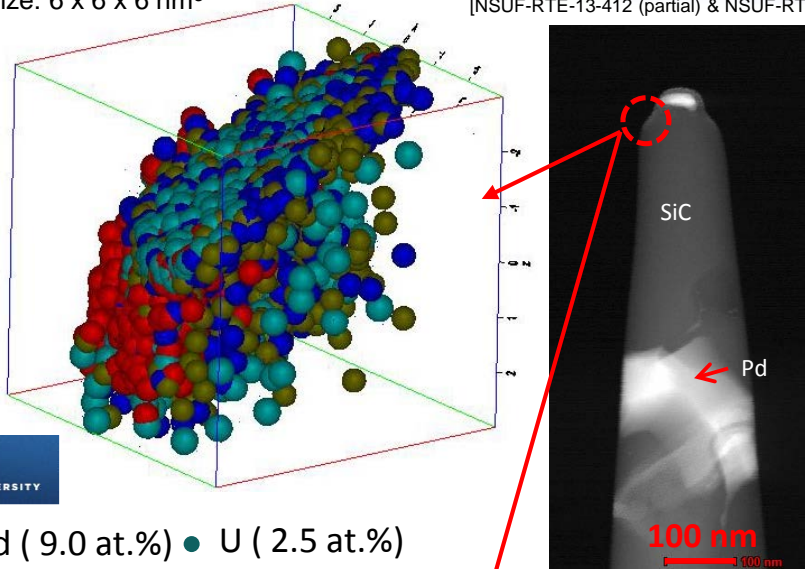
Non-homogeneous distribution of Fission Products

Volume size: 6 x 6 x 6 nm³

[NSUF-RTE-13-412 (partial) & NSUF-RTE-14-541]

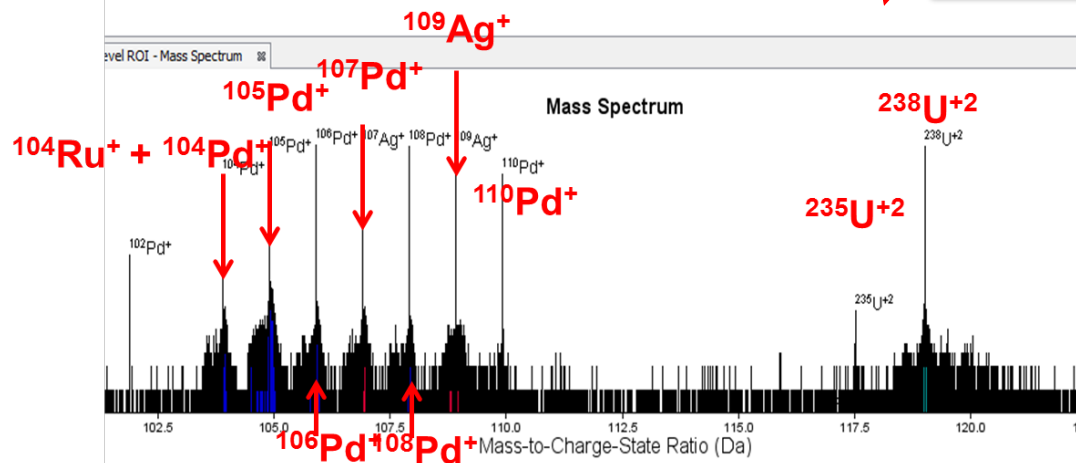
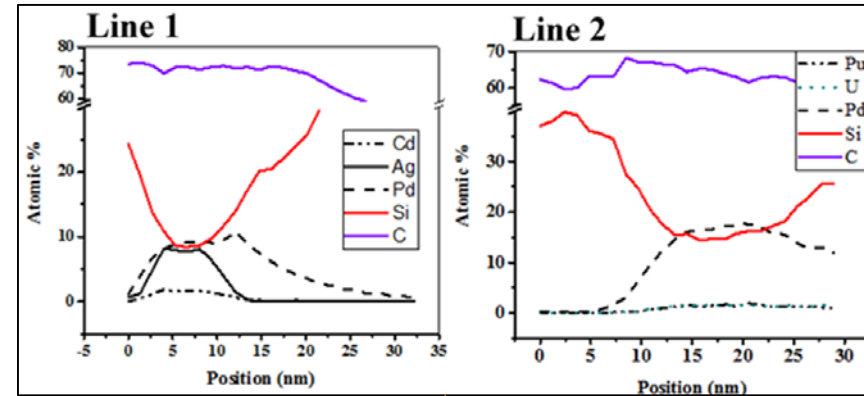
AGR2-223-RS06

AGR1-632-034

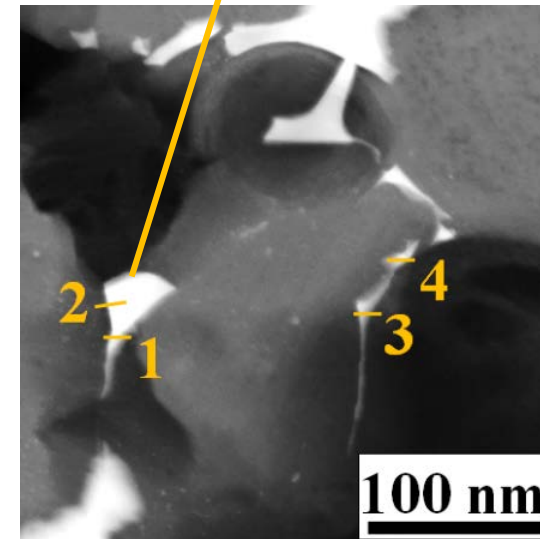


- Pd (9.0 at.%) ● U (2.5 at.%)
- Ag (2.7 at.%) ● Ru (0.4 at.%)

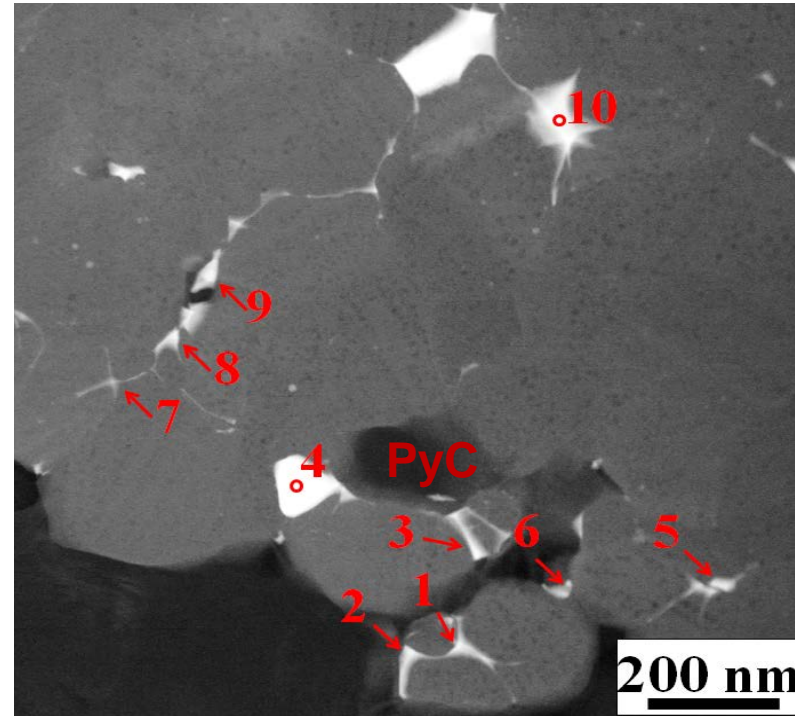
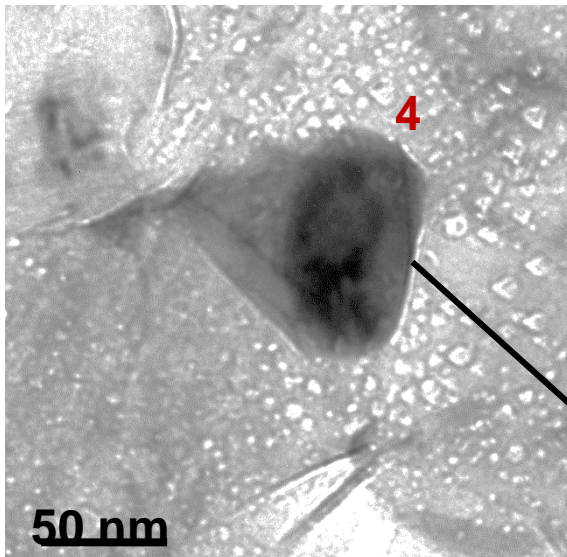
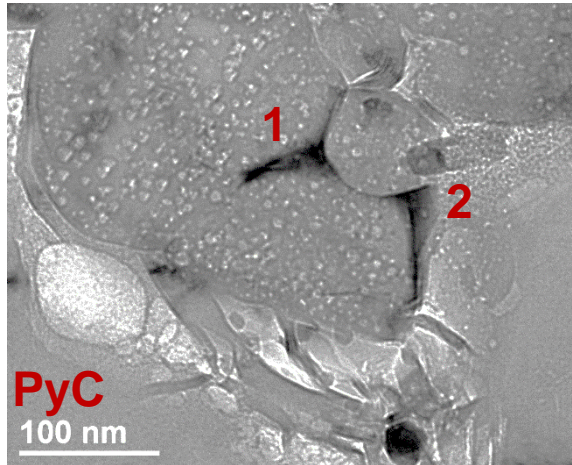
Irradiated SiC APT tip



Indexed based on physics predictions of isotopic inventory

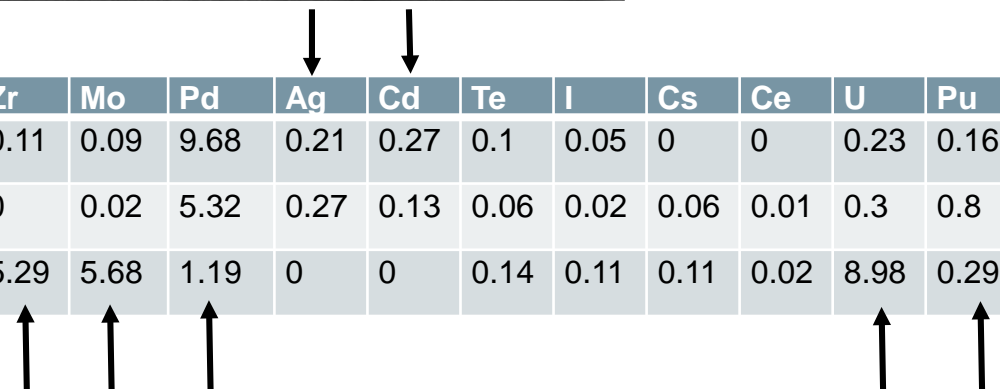


Difference in composition between nano- and micron precipitates

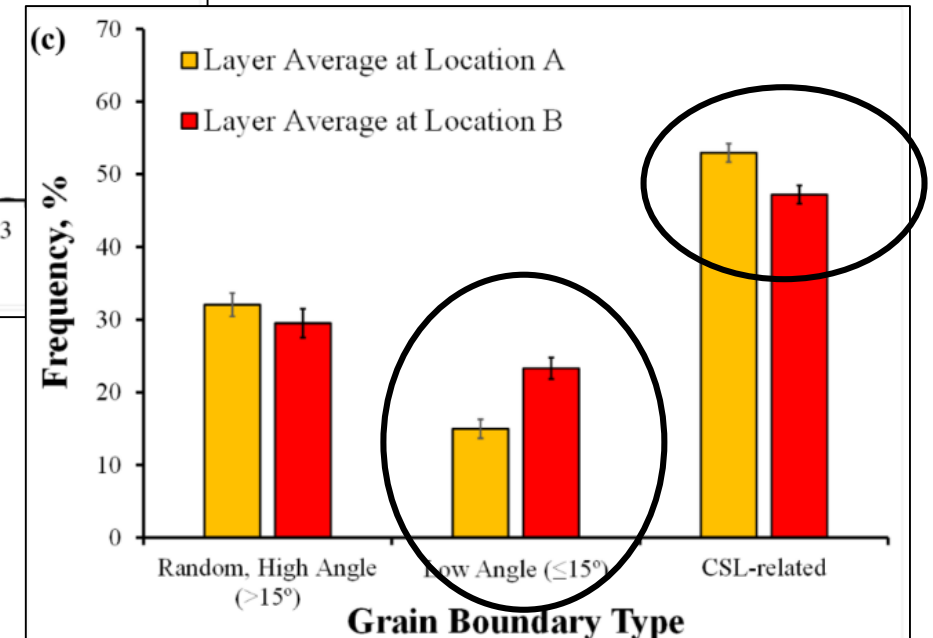
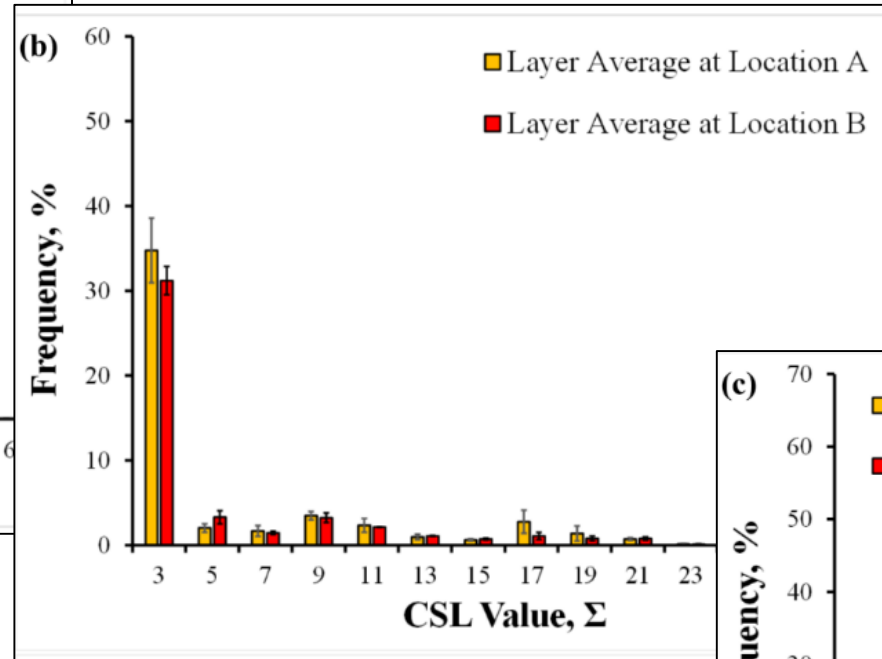
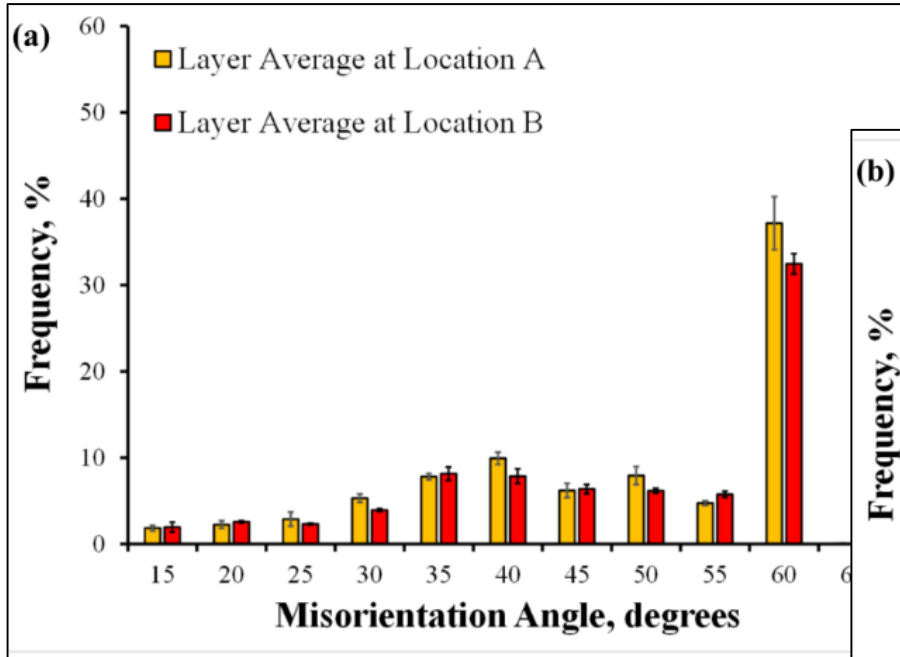
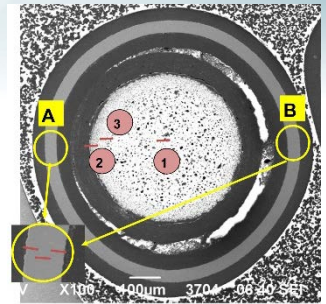


AGR2-223-RS06
Lamella 10

	Si	C	Zr	Mo	Pd	Ag	Cd	Te	I	Cs	Ce	U	Pu
P-1	41.25	47.79	0.11	0.09	9.68	0.21	0.27	0.1	0.05	0	0	0.23	0.16
P-2	35.18	57.76	0	0.02	5.32	0.27	0.13	0.06	0.02	0.06	0.01	0.3	0.8
P-4	14.04	64.1	5.29	5.68	1.19	0	0	0.14	0.11	0.11	0.02	8.98	0.29



AGR-2 Grain Boundary Characteristics: Compare A and B

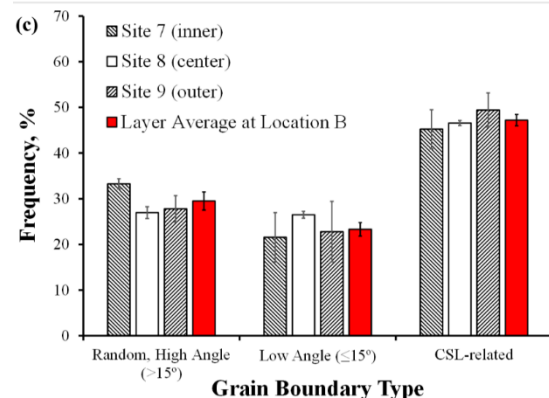
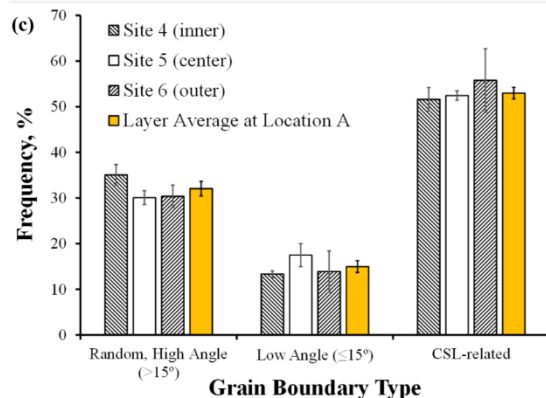
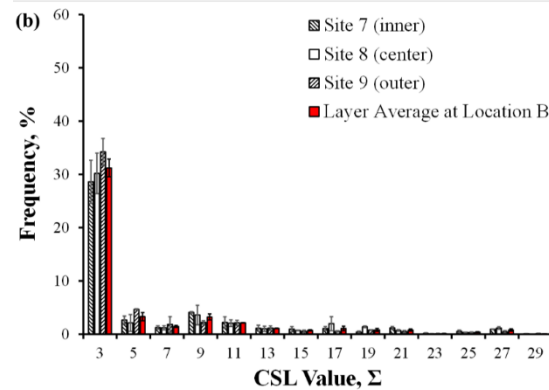
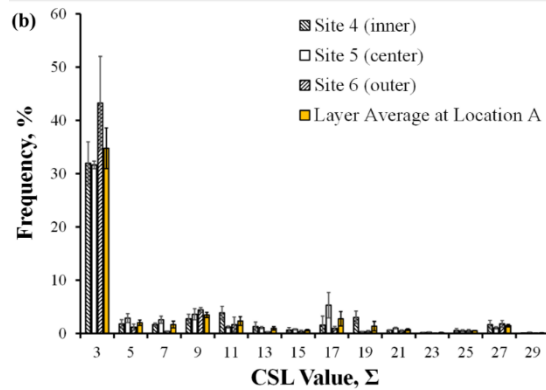
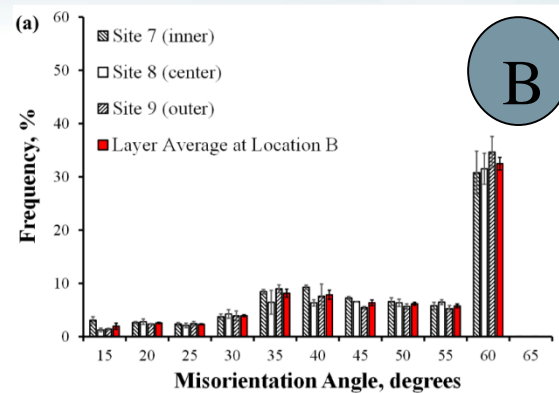
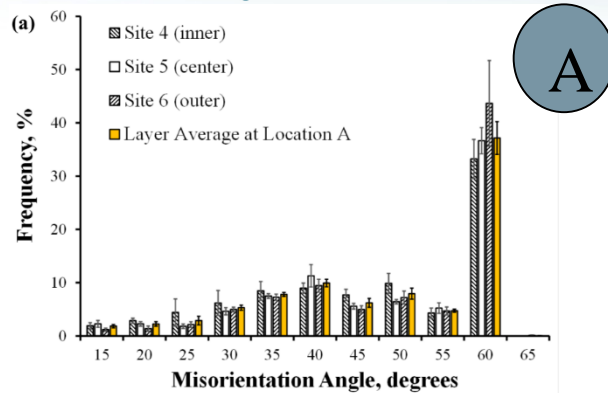
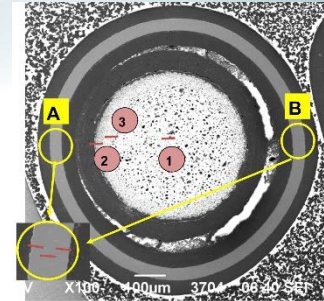


Location B tends to have a statistically:

- higher fraction of low angle grain boundaries
- lower fraction of CSL-related grain boundaries compared to Location A..

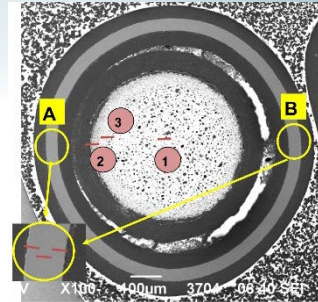


Grain boundary distributions: Locations A and B

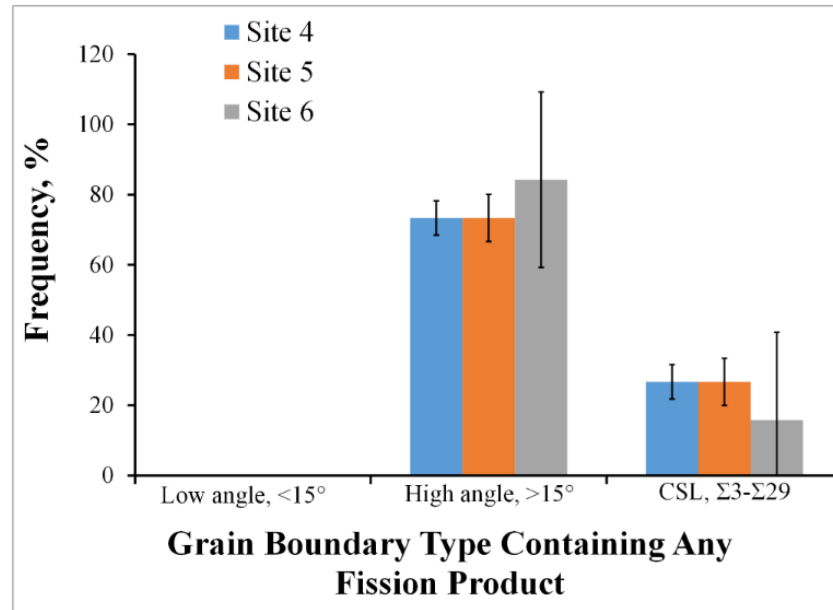


No statistically significant differences noted in the SiC grain boundary distributions at inner, central and outer regions of the SiC layer at each location analyzed.

Fission Product Grain Boundary Precipitate Summary: Area A

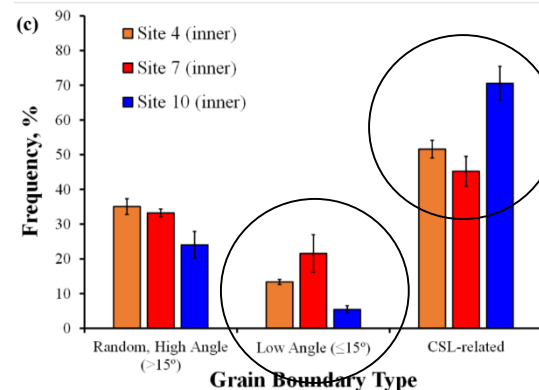
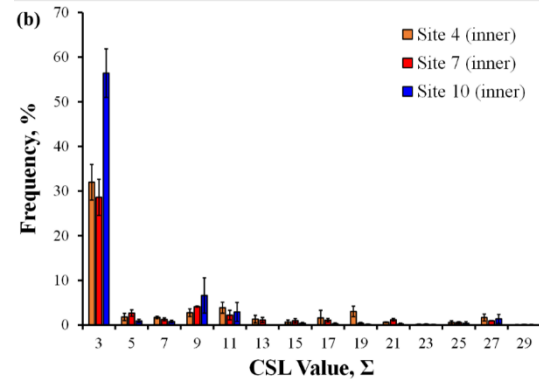
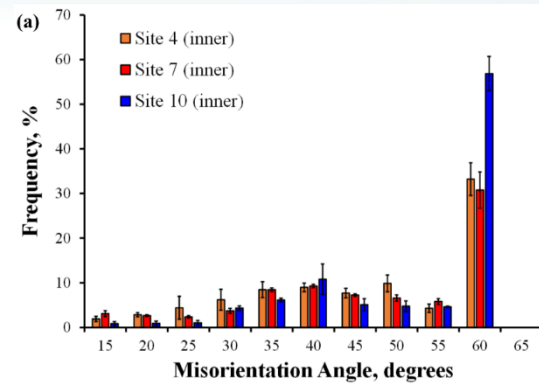
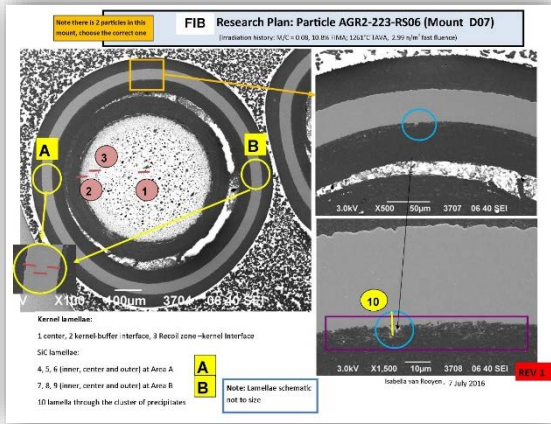


AGR2-223-RS06



- No fission products on low angle grain boundaries
- Precipitates prefer random, high angle grain boundaries
- The distribution between random, high angle and CSL-related grain boundaries is statistically the same across the SiC layer
- Precipitates contain mainly Pd and U –(Ag was not found in any grain boundary precipitate)
- Mo was found in some of the larger precipitates of AGR2-223-RS06

Grain boundary characteristics of all inner layer areas examined



Generally, the trends in the SiC grain boundary distributions at each location are similar. However, there are statistically significant differences in the fractions of the CSL-related and low angle grain boundaries in these two locations but they are relatively small.

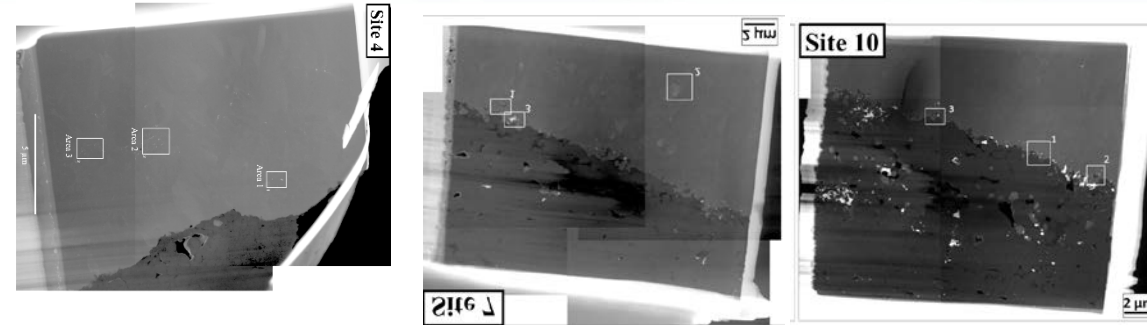
Additional inner region, exhibiting a cluster of fission product precipitates, showed a significantly higher fraction of CSL-related grain boundaries and lower fractions of low angle and random, high angle grain boundaries than in either of the other two locations.

The reason for difference in the SiC grain boundary distribution in the region with the cluster of fission product precipitates, and whether this was a factor in the development of the fission product precipitate cluster, is unknown at this time.

Location-dependent Grain Boundary Distribution characteristics

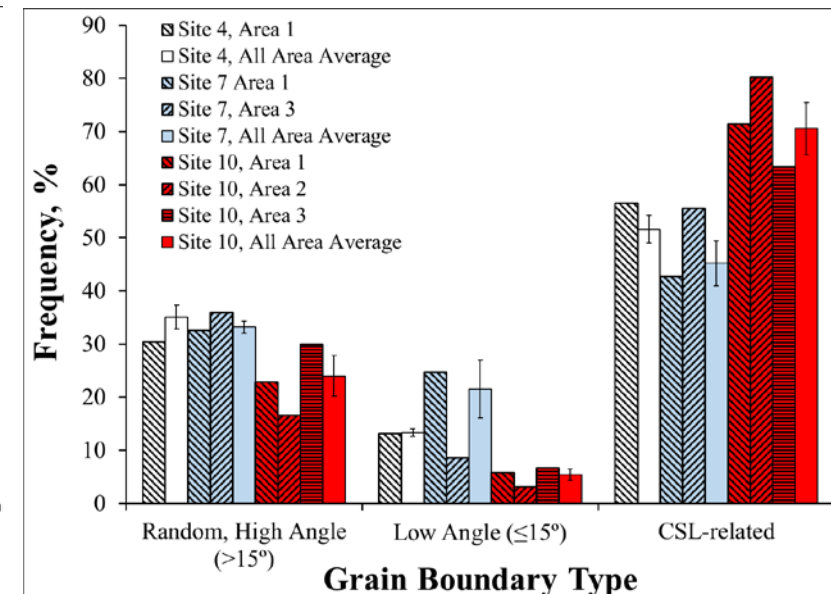
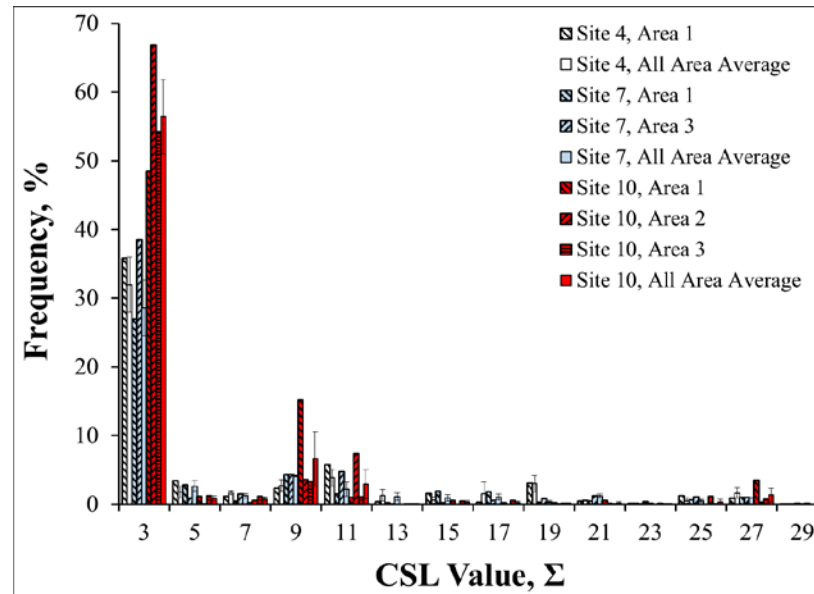
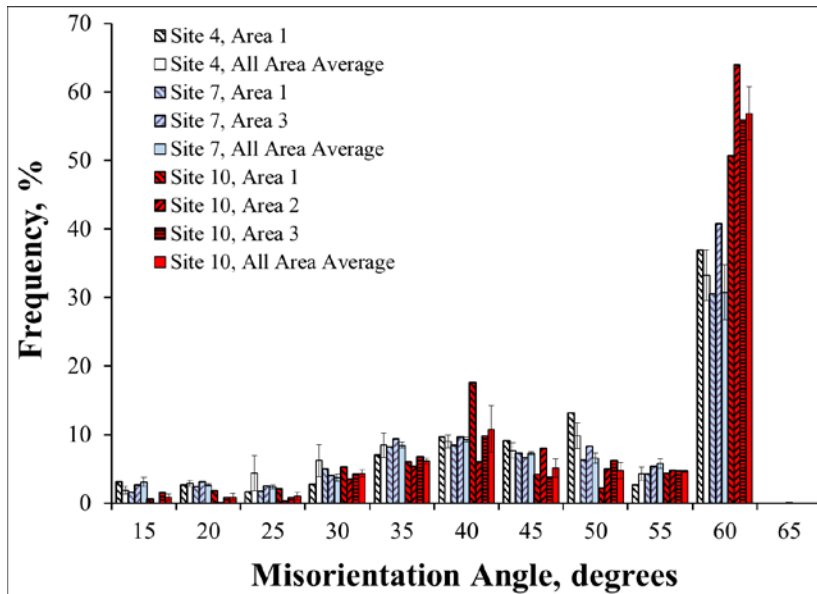
Analysis locations at each site

- All areas on Site 10 were **on** the IPyC interface
- Only Area 1 on Site 4 was near the interface (~1 μ m)
- Only Areas 1&3 on Site 7 were near the IPyC interface (<0.5 μ m)

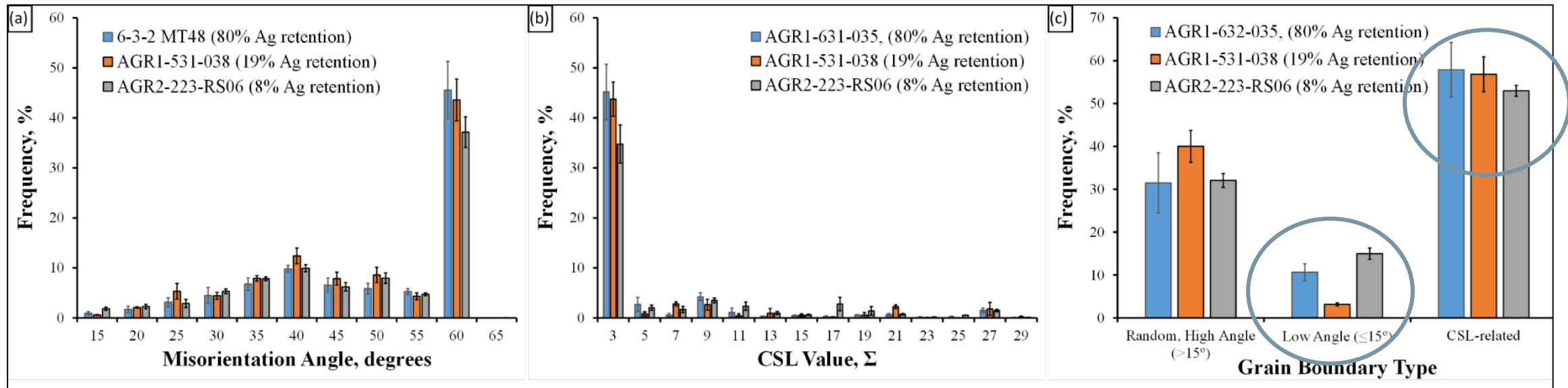


Comparison of distributions only near the IPyC interface

- Generally, the differences between Site 10 and the others are less
- Grain boundary distributions still show significant differences at Site 10 compared to Sites 4 & 7



Comparison to AGR-1 TRISO Particles



- AGR2-223-RS06 has a lower fraction of $\Sigma 3$ grain boundaries and overall fraction of CSL-related grain boundaries than the AGR-1 particles
- A high random, high angle grain boundary fraction is not exhibited by the high release AGR-2 particle as was found with the AGR-1 particles (increasing random, high angle grain boundary fraction correlated with increasing Ag-110m release) – but need to compare the high Ag-110m release SiC distribution found in AGR2-223-RS0-6 to a low Ag-110m release, AGR-2 TRISO particle
- Low angle grain boundary fraction of AGR2-223-RS06 is higher than in AGR-1 TRISO particles

Kernel & Kernel-Buffer interlayer: Scope and Matrix

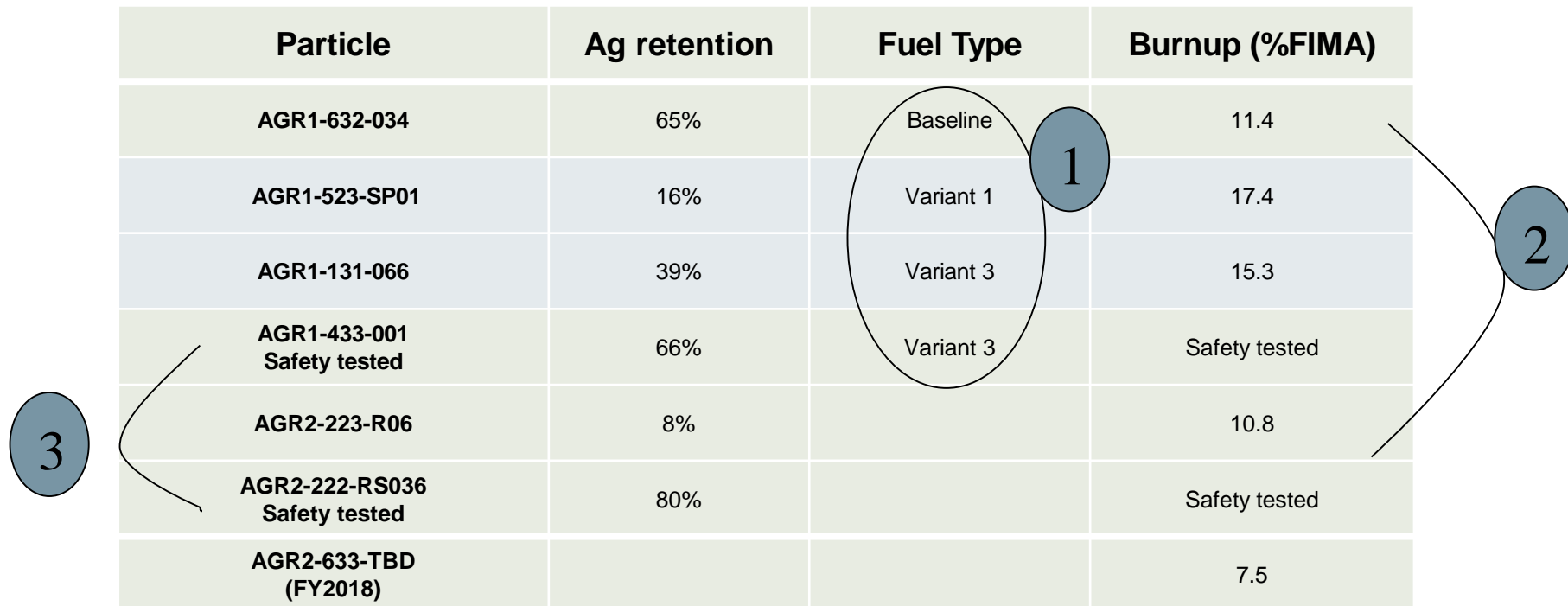
What?

- fission product precipitate location,
- chemical composition of fission product precipitates and fuel kernel, micro-and nanostructures.

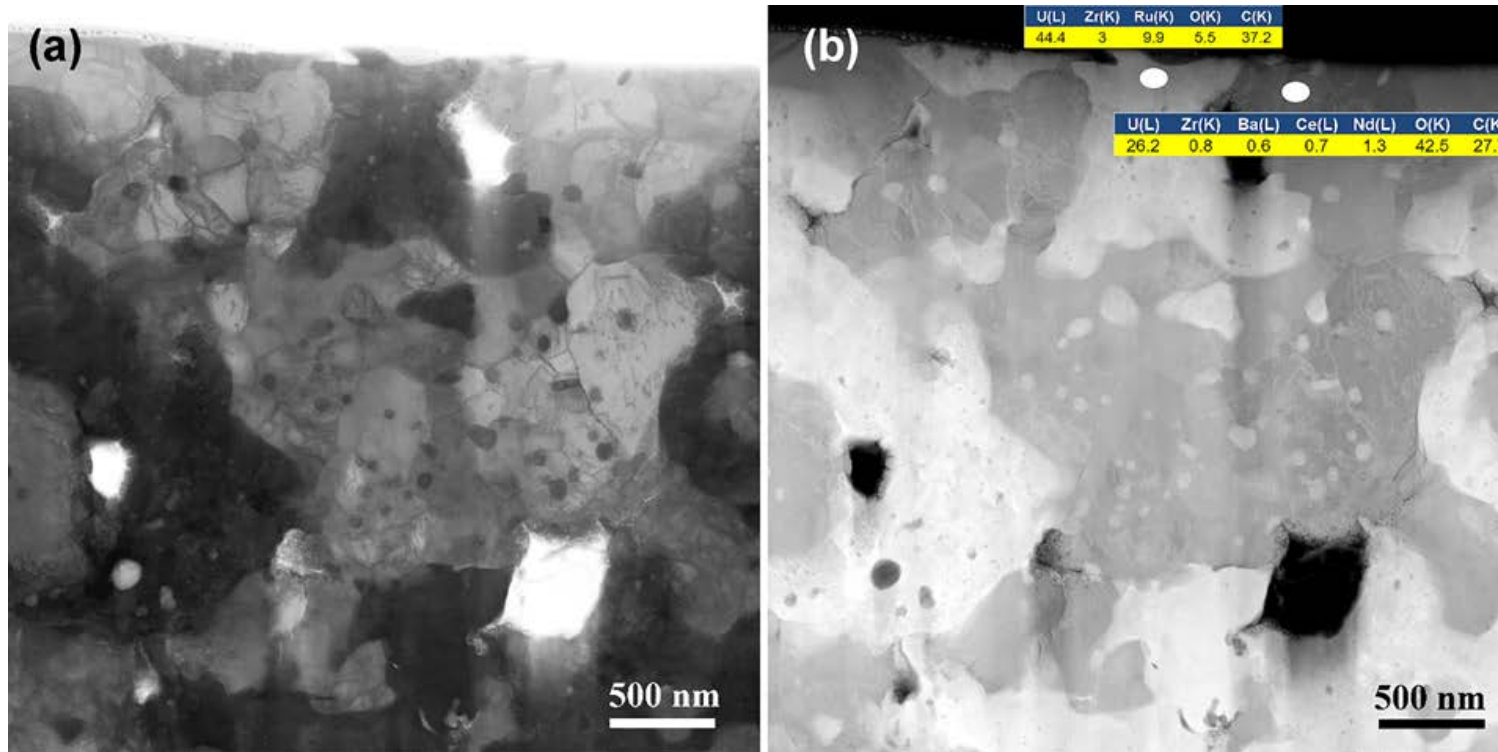
Why?

- 1: effect of fuel type and burnup
- 2: effect of lab scale vs pilot scale (approx. same burnup)
- 3: comparison of AGR-1 vs AGR-2 safety tested kernel

Particle	Ag retention	Fuel Type	Burnup (%FIMA)
AGR1-632-034	65%	Baseline	11.4
AGR1-523-SP01	16%	Variant 1	17.4
AGR1-131-066	39%	Variant 3	15.3
AGR1-433-001 Safety tested	66%	Variant 3	Safety tested
AGR2-223-R06	8%		10.8
AGR2-222-RS036 Safety tested	80%		Safety tested
AGR2-633-TBD (FY2018)			7.5



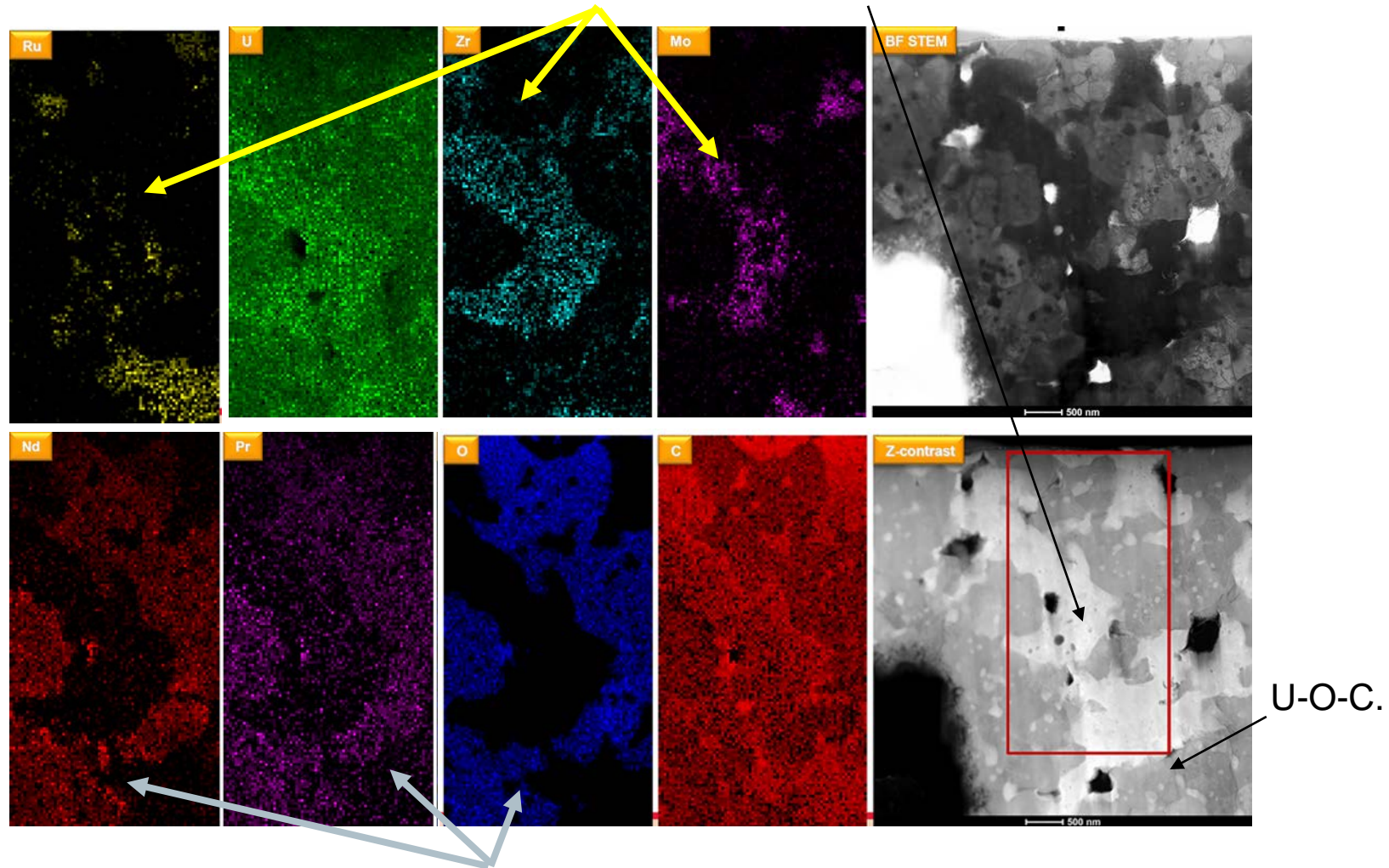
Kernel Examination: Preliminary Results



AGR1-131-066

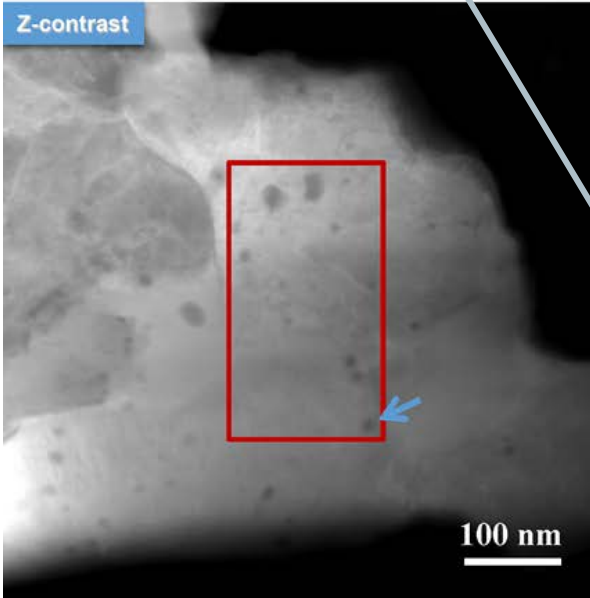
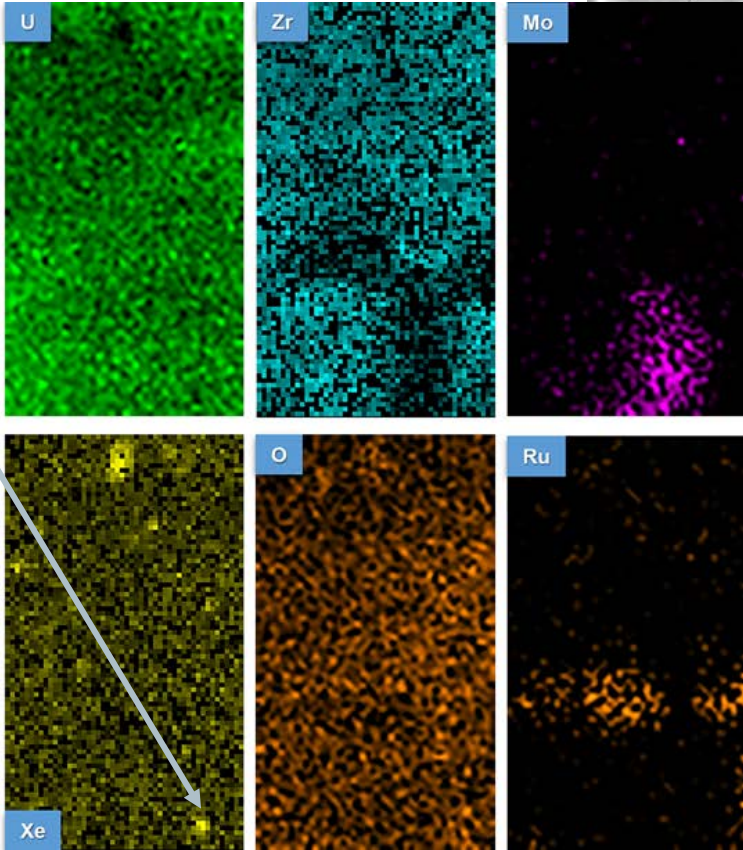
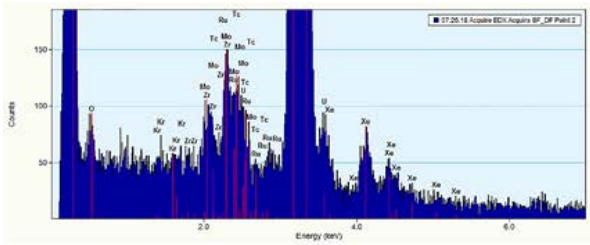
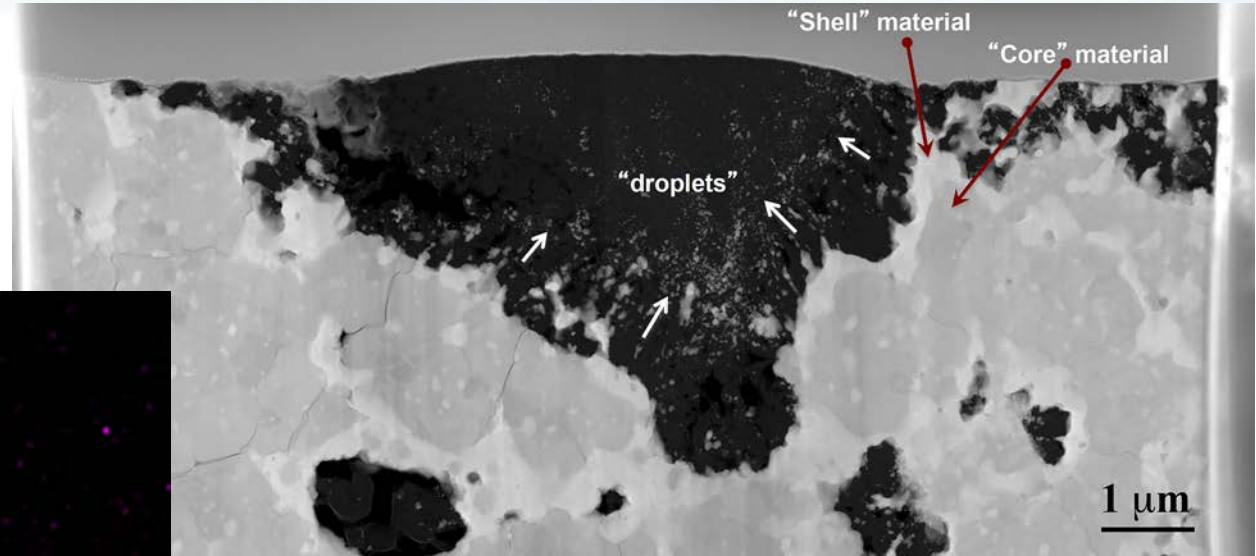
AGR1-131-066 (EDS spectral images of the two-phase structure)

Zr, Mo, Ru, Tc residing primarily in the high Z phase

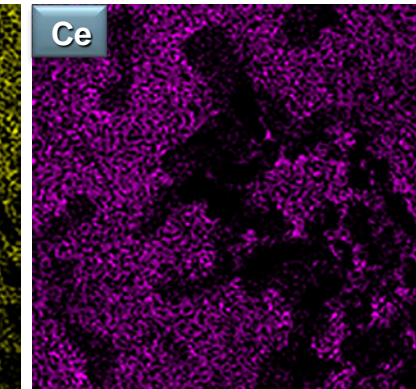
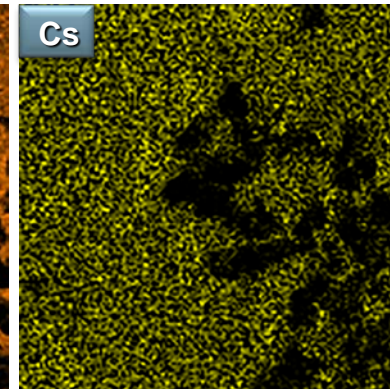
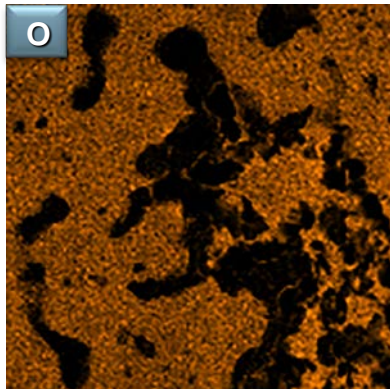
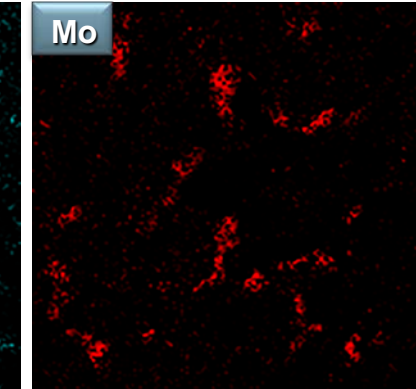
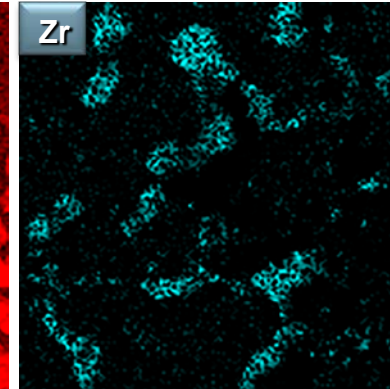
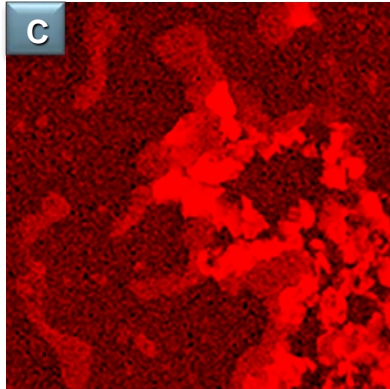
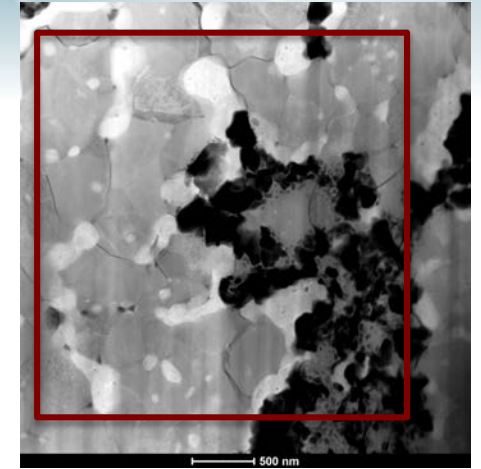
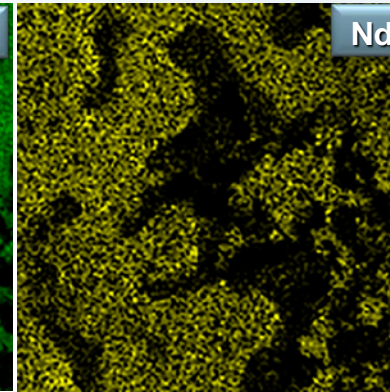
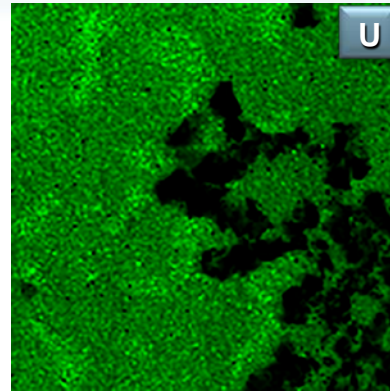
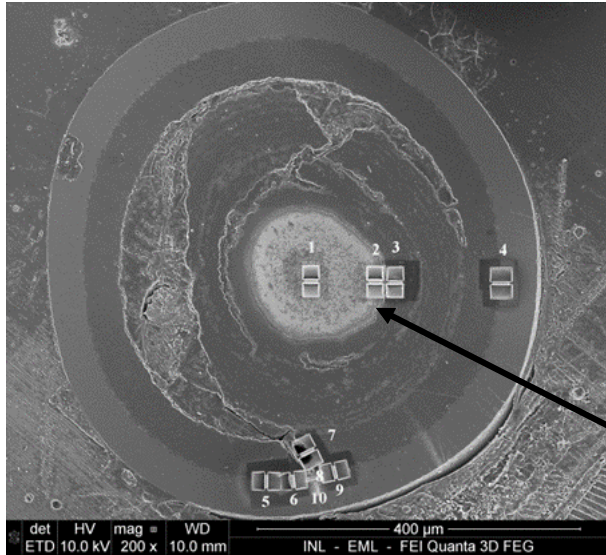


Nd, Pr, and O are found primarily in the U-O-C.

Buffer / fuel kernel interface area AGR1-131-066

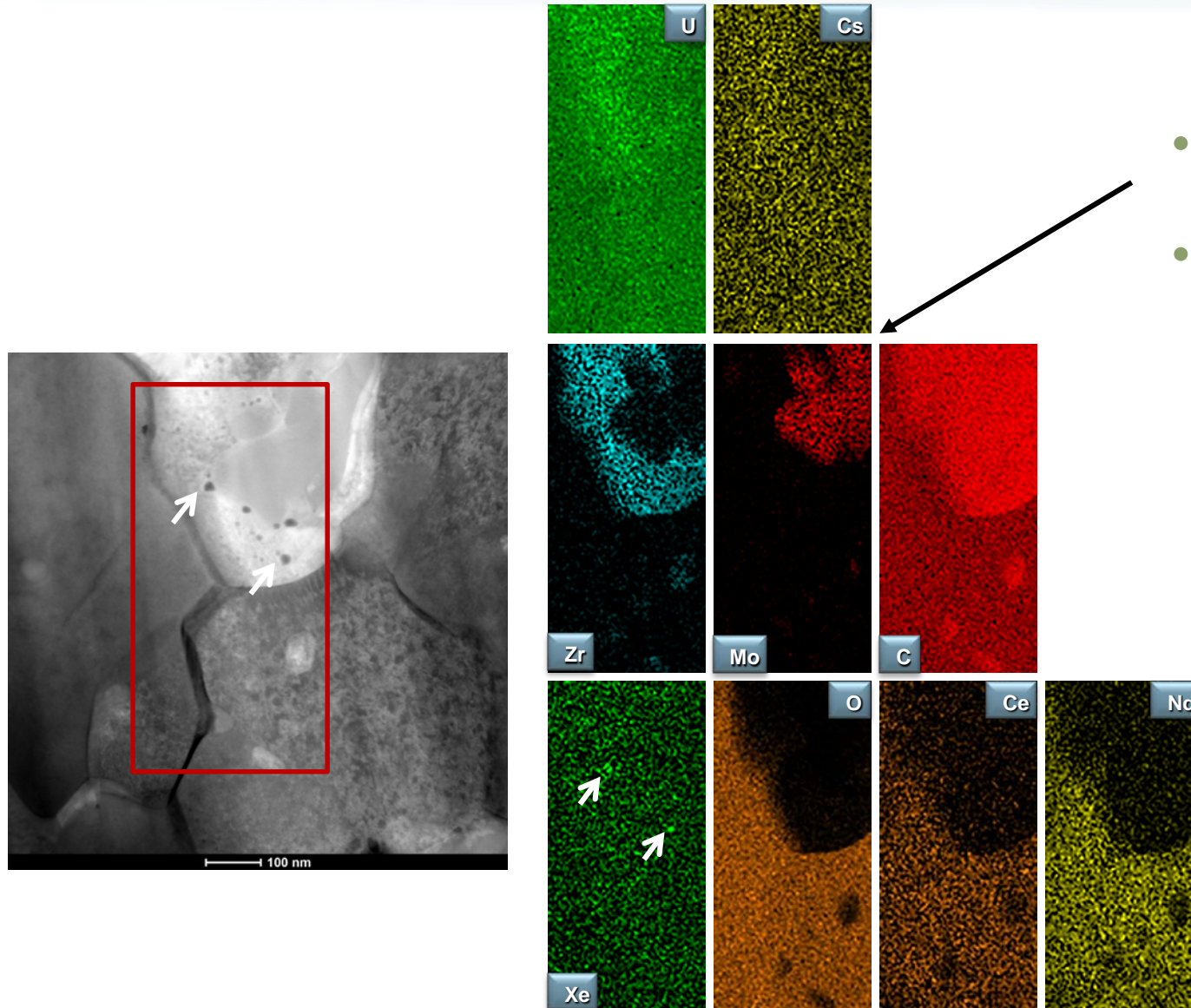


Kernel: Particle AGR1-532-SPO1 Lamella 2



- Map of the area indicated below.
- C present in the “pore” areas likely came from metallographic mounting process, from which the FIB specimen was taken.

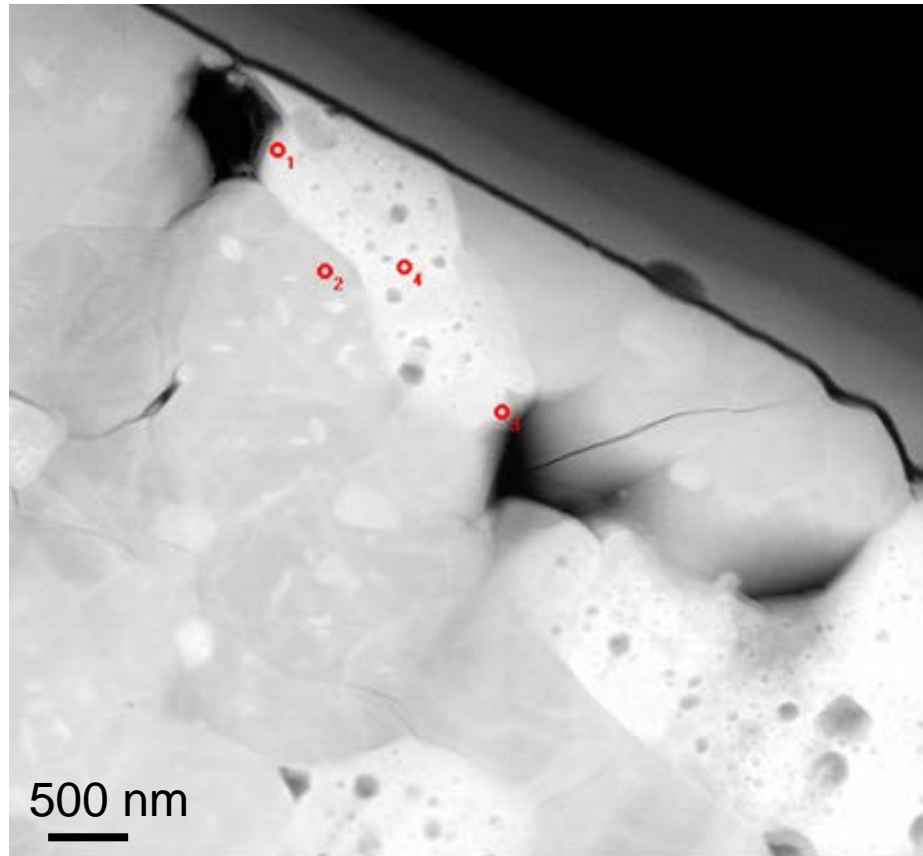
Kernel: Particle AGR1-532-SPO1 Lamella 2



- Segregation of the Zr, Mo, (and Ru) in the carbide phase.
- Nd, Ce, Cs present at low levels.

Kernel Particle AGR2-223-R06 Lamella 1

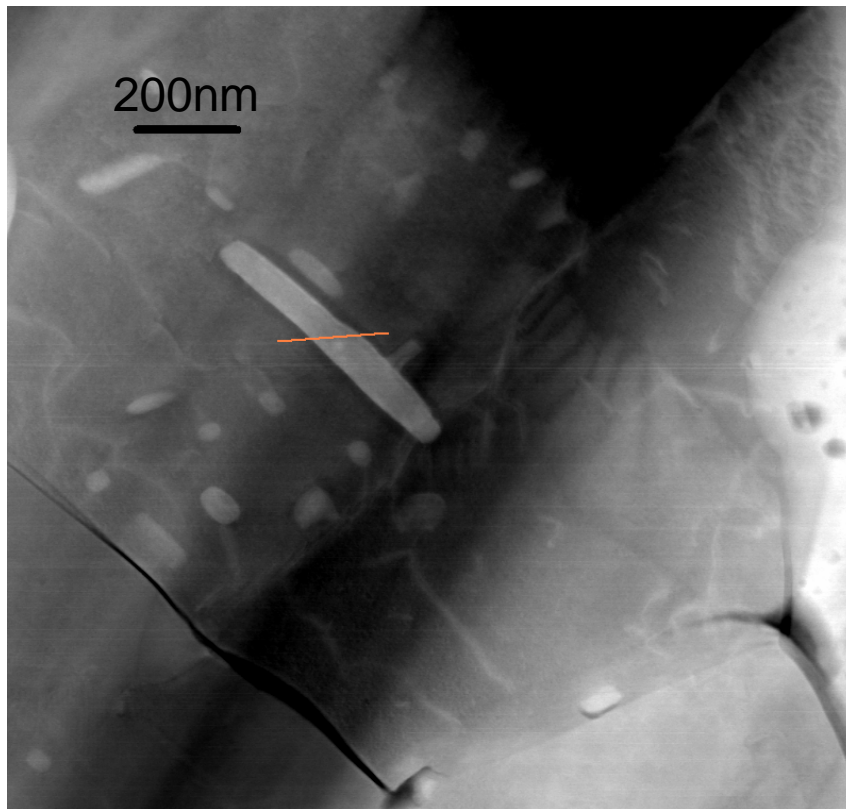
Location Picture



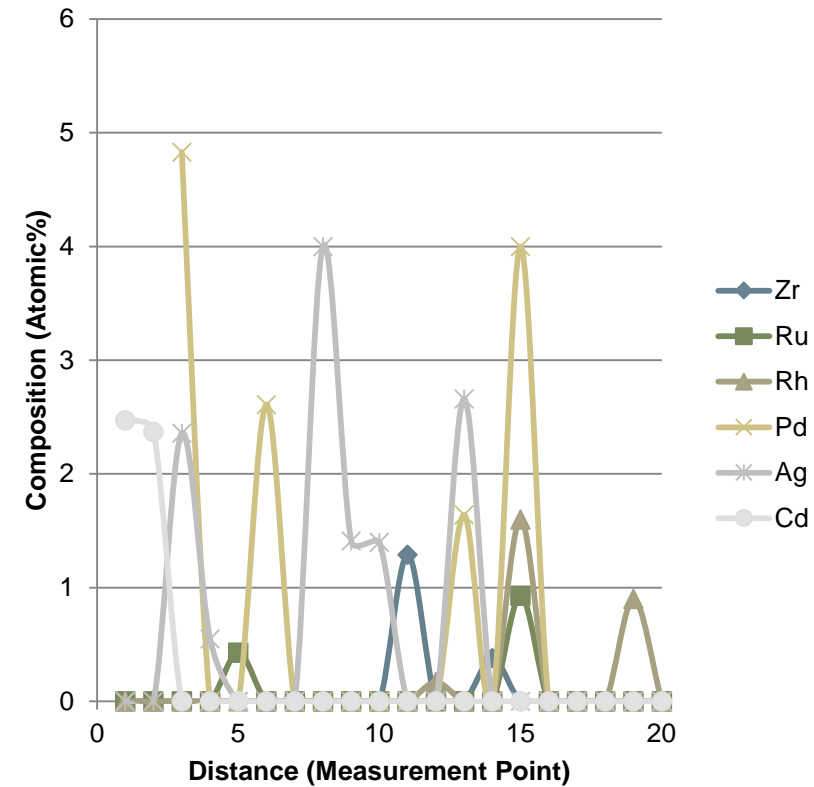
Composition Table (Atomic%)

Element	Location 1	Location 2	Location 3	Location 4
Zr	9.83	1.24	7.96	10.82
Ru	0.29	0.53	0.06	0.29
Rh	0.00	0.00	0.00	0.00
Pd	0.00	0.00	0.00	0.00
Ag	0.08	0.00	0.00	0.00
Cd	0.00	0.00	0.00	0.00
U	89.79	98.22	91.96	88.87

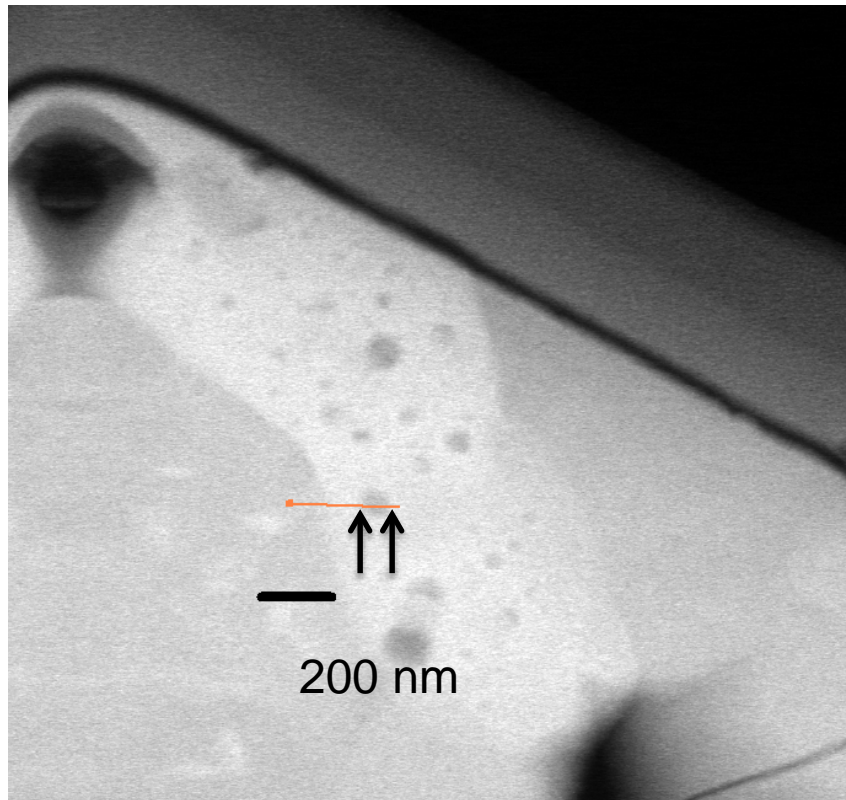
Kernel Particle AGR2-223-R06 Lamella 1



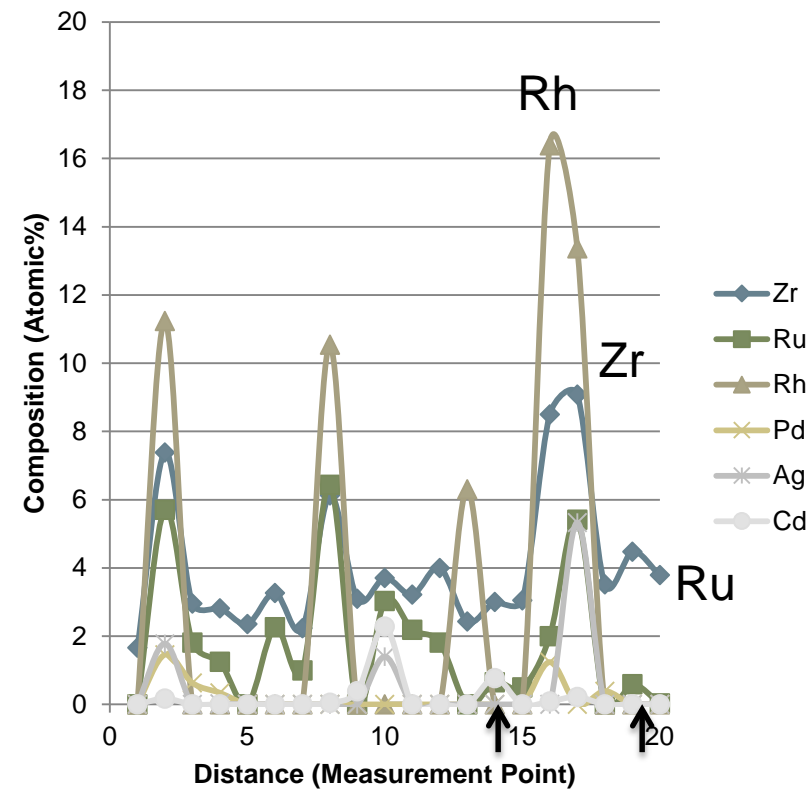
Line Scan Composition



Kernel Particle AGR2-223-R06 Lamella 1



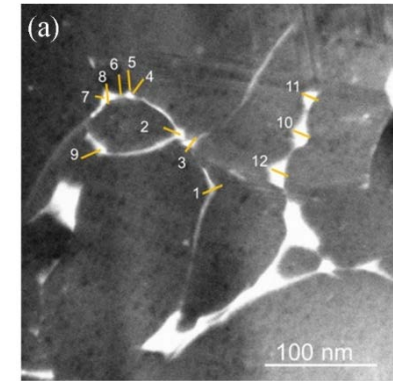
Line Scan Composition



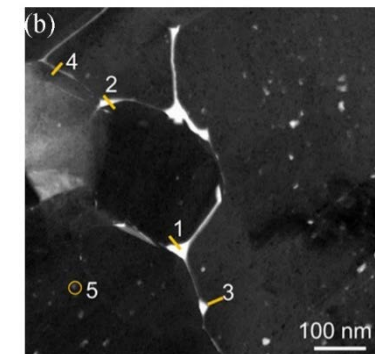
Preliminary Thermodynamic Study 4

- Simple Solid Solution
- Intermetallic + Solid Solution & Simple Transformation
- Intermetallic + Solid Solution & Complex Transformation

#	Fission Products Atomic %	Pd	Ag	Cs	Ce	Eu	U	Pu	Phase	Crystal Structure Transformation Scheme	Phase Change Temperature, °C	Pearson Symbol	Space Group
Area 1													
1	1.29	96.90	0.00	0.00	0.00	0.00	0.00	3.10	(Pd,Pu)	FCC	1500	cF4	Fm $\bar{3}$ m
2	0.48	100	0.00	0.00	0.00	0.00	0.00	0.00	Pd	FCC	1555	cF4	Fm $\bar{3}$ m
3	1.10	100	0.00	0.00	0.00	0.00	0.00	0.00	Pd	FCC	1555	cF4	Fm $\bar{3}$ m
4	1.66	45.78	54.22	0.00	0.00	0.00	0.00	0.00	(Pd,Ag)	FCC	1265	cF4	Fm $\bar{3}$ m
5	0.74	43.24	56.76	0.00	0.00	0.00	0.00	0.00	(Pd,Ag)	FCC	1248	cF4	Fm $\bar{3}$ m
6	0.12	100	0.00	0.00	0.00	0.00	0.00	0.00	Pd	FCC	1555	cF4	Fm $\bar{3}$ m
7	1.15	59.13	40.87	0.00	0.00	0.00	0.00	0.00	(Pd,Ag)	FCC	1326	cF4	Fm $\bar{3}$ m
8	0.13	100	0.00	0.00	0.00	0.00	0.00	0.00	Pd	FCC	1555	cF4	Fm $\bar{3}$ m
9	1.45	40.00	0.00	0.00	58.62	0.00	1.38	0.00	Ce ₃ (Pd,U) ₂	Rhombohedral	1037		P $\bar{3}$?
10	1.13	83.19	0.00	0.00	0.00	0.00	13.27	3.54	(U,Pu)Pd ₄ + (U,Pu)Pd ₈ or Pd(U,Pu)	Simple Cubic + ?<700°C<FCC	Pd(U,Pu) Melting 1300 & (U,Pu)Pd ₈ Decomp 800 (U,Pu)Pd ₄ Melt 1585	cF4, ? & cP4	Fm $\bar{3}$ m, ? & Pm $\bar{3}$ m
11	2.31	100.00	0.00	0.00	0.00	0.00	0.00	0.00	Pd	FCC	1555	cF4	Fm $\bar{3}$ m
12	1.51	9.93	90.07	0.00	0.00	0.00	0.00	0.00	(Pd,Ag)	FCC	1025 Melt	cF4	Fm $\bar{3}$ m
Area 2													
1	5.57	65.17	0.00	0.00	0.00	0.00	34.83	0.00	UPd ₃ + U	Hexagonal + Monoclinic	1640	hP16	P6 ₃ /mmc
2	5.07	99.21	0.00	0.00	0.00	0.00	0.79	0.00	(Pd,U)	FCC	1550	cF4	Fm $\bar{3}$ m
3	2.89	85.12	0.00	0.00	0.00	0.00	12.46	2.42	(U,Pu)Pd ₄ + (U,Pu)Pd ₈ or (Pd,U,Pu)	Simple Cubic + ?<700°C<FCC	Pd(U,Pu) Melting 1300 & (U,Pu)Pd ₈ Decomp 800 (U,Pu)Pd ₄ Melt 1585	cF4, ? & cP4	Fm $\bar{3}$ m, ? & Pm $\bar{3}$ m
4	2.24	92.41	5.36	0.00	0.00	0.00	2.23	0.00	(Pd,Ag,U)	FCC	1500	cF4	Fm $\bar{3}$ m
5	0.28	71.43	0.00	0.00	0.00	0.00	21.43	7.14	(U,Pu)Pd ₃ + (U,Pu) or (U,Pu) ₅ Pd ₆	Hexagonal + ($\alpha \rightarrow \beta \rightarrow \gamma \rightarrow U_3Pd_6$)	1640, 970 & 1110	hP16 & (oC4 \rightarrow tP30 \rightarrow cI2 \rightarrow ?)	P6 ₃ /mmc & (Cmcm \rightarrow P4 ₂ /mmm \rightarrow I m $\bar{3}$ m \rightarrow ?)



Precipitates from inner area of the SiC layer from TRISO particle AGR1-632-035 (a) Area 1 and (b) Area 2



Publications/Reports/Presentations

Completed/Submitted FY2017 INL papers/reports:

- H. Wen and I.J. van Rooyen, Distribution of fission products palladium, silver, cerium and cesium in the un-corroded areas of the locally corroded SiC layer of a neutron irradiated TRISO fuel particle, <http://dx.doi.org/10.1016/j.jeurceramsoc.2017.04.012>.
- T. M. Lillo, I. J. van Rooyen, and J. A. Aguiar, Silicon carbide grain boundary distributions, irradiation conditions and silver retention in irradiated AGR-1 TRISO fuel particles. Special NED issue devoted to the best of HTR2016.

Presentations FY2017

- Isabella J van Rooyen, Advanced microscopy and Micro-analysis results: Neutron Irradiated AGR TRISO fuel, TCT meeting 18 May 2017 Idaho Falls.
- I. J. van Rooyen, C. Parga, J. Rosales, T.M. Lillo and K. Wright (Presented by P. Demkowicz), Fission product composition and distribution in SiC layers of neutron irradiated AGR-1 TRISO Fuel, Baotou China, 4th SiC workshop
- E J Olivier, J H Neethling, I J van Rooyen, Cs-corrected STEM and EDS Investigation of Pd and Ag transport along SiC grain boundaries and dislocations, Baotou China, 4th SiC workshop

Publications/Reports/Presentations

Possible FY2017 INL papers/reports:

- S Meher, IJ van Rooyen, TM Lillo, "Metamorphosis in crystalline solids under neutron irradiation", Journal paper, to be submitted July 2017
- IJ van Rooyen, S Meher, T Lillo, K Wright, Advanced microscopy examination on Particle AGR2-223-RS06, INL external report to be submitted for internal review October 2017
- FY2017 progress report on AGR2 particle microstructure, kernel examination and neutron irradiation damage effects

Possible future collaborative papers:

- J Olivier, J Neethling, I J van Rooyen, Cs-corrected STEM and EDS Investigation of Pd and Ag Transport Along SiC Grain Boundaries and Dislocations, to be submitted September 2017
- M Cook, IJ van Rooyen, Y Yang, STEM characterization of neutron irradiated UCO kernels, to be submitted September 2017

Collaborations FY2017

- Submit a NSUF RTE fund application with University of Florida: Project PIs: Yong Yang, Isabella van Rooyen, Mukesh Bachhav, Graduate Student Team Member: Matthew Cook,
 - Characterize the Irradiated Microstructure and Understand the Fission Product Behavior in an Irradiated AGR-1 TRISO Fuel Particle Kernel.
- Subcontract with University of Florida: Prof Yong Yang, PhD candidate Matthew Cook
 - Effects of Neutron Irradiation on the Micro/Nano Scale Structure and Fission Product Distribution of TRISO Coated Particle Fuel Kernels from AGR Experiments
- Summer/Fall 2016 Part time Intern University of Florida: Jhonathan Rosales
 - AGR-1 Fission product element combinations
- Nelson Mandela Metropolitan University, Jan Neethling and Jaco Olivier: Joint presentation at SiC workshop

Conclusions

- Shakedown based on AGR-1 particles provided basis applied to continued work on AGR-2 particles
- Effect of gap between layers on fission product distribution were identified for AGR-2 particle:
 - Sr, Eu in RZ significantly higher (4x) in non-gap size vs gap size
 - Xe: peak in RZ (non-gap) vs in kernel (gap)
 - Cs and I: not affected by gap between layers
- AGR-2 particle seems to contain higher Mo concentration in micron-sized precipitates.
- Kernel examination: seems preferred presence in different fuel phases (segregation of Zr, Mo, (and Ru) in carbide phase).
- Significant difference in low angle boundaries at different locations in inner area (fission product clustering) in AGR-2 particle.
- Low angle grain boundary fraction of AGR2-223-RS06 is higher than in AGR-1 TRISO particles.
- Strengthened collaborations and establish new collaborations which enhanced quality of results.

Recommendations: Future Work

- Data mining AGR-1 results
 - Integrate grain boundary characteristics, neutron damage, chemical composition and structural information for fission product mechanisms
 - Re-examine Grain boundary characteristics results:
 - redefine the distance classifications to micron and determine if this relate to different trends
 - Representativeness of areas chosen
 - Compare location and composition obtained from micro and nano scale measuring tools
- Explore In-situ high temperature TEM transport studies
 - Use current lamellae if possible (minimize FIB preparation time)
 - Current stages up to 1100°C (Determine possible higher temperature TEM stages)
 - Examine both micron size and grain boundary precipitates
- Expand the neutron damage work currently performed (proposal available)



- Understand the onset of transport, therefore improving the potential for improving predicting models
- Resulting in designing better fuels

Contribution Towards Program Goals

- **Improve understanding of TRISO fuel behavior** based on observed and measured phenomena that affect fuel performance and fission product release.
- **Fission product interactions** with layers and potential degradation of properties (property needs) p46
- 12/24/15 email from Jack Simonds: quote from the NRC review of NGNP/AGR white papers submitted that drives the need for advanced microscopy of the AGR TRISO fuel particles in anticipation of future NRC licensing by an applicant.
- “The staff acknowledges that the AGR Fuel Program includes significant ongoing and planned research efforts to investigate the poorly understood phenomenology of silver and palladium interactions with TRISO coating layers. DOE/INL has stated that these research efforts may include examinations on fuel samples irradiated in the ATR at temperatures significantly above those normally expected during irradiation in an NGNP core. The staff would consider new insights emerging from such investigations in evaluating the potential fuel performance uncertainties associated with the initially unmet need for test data from real-time fuel irradiations in an HTGR neutron spectrum.”

Not full list

Acknowledgements

- Scott Ploger and Jason Harp: Mount and decontamination preparation for electron microscopy examination and micro-analysis
- Jim Madden: FIB-STEM and APT sample preparation
- Terry Holesinger (LANL): HRTEM, STEM, kernel

This work was sponsored by the U.S. Department of Energy's Office of Nuclear Energy, under U.S. Department of Energy Idaho Operations Office Contract DE-AC07-05ID14517, as part of the Advanced Reactor Technology Program and the Nuclear Scientific Users Facility–Rapid Turnaround Experiments program.

Questions??

Isabella van Rooyen

Isabella.vanrooyen@inl.gov

Idaho National Laboratory

(208) 526-4199



Ready for
lunch !!!



Idaho National Laboratory

Extra slides

Technique Acronyms

Acronyms	Description
APT	Atom Probe Tomography
EDS	Energy Dispersive Spectroscopy
EBSD	Electron Back Scattered Diffraction
EELS	Electron Energy Loss Spectroscopy
EFTEM	Energy Filtered TEM
EPMA	Electron Probe Micro-Analysis
FIB	Focused Ion Beam
HRTEM	High Resolution Transmission Electron Microscopy
SAD	Selected Area Diffraction
SEM	Scanning Electron Microscope
STEM	Scanning Transmission Electron Microscopy
TEM	Transmission Electron Microscope
<i>t</i> -EBSD	Transmission-EBSD
TKD	Transmission Kikuchi Diffraction
WDS	Wavelength Dispersive Spectroscopy

Results: irradiated TRISO

Physics predictions of the isotopic inventory in the specimen

AGR-1 Compact 6-3-2	decay time after the end of irradiation				Atomic Mass
Isotope	0-days	1-day	1-yr	2-yrs	
PD104	2.46E-06	2.46E-06	2.46E-06	2.46E-06	104
RU104	1.06E-05	1.06E-05	1.06E-05	1.06E-05	104
PD105	6.13E-06	6.15E-06	6.18E-06	6.18E-06	105
RH105	4.23E-08	3.12E-08	0	0	105
RU105	6.71E-09	1.64E-10	0	0	105
PD106	2.49E-06	2.49E-06	3.65E-06	4.23E-06	106
RH106	4.21E-12	2.18E-12	1.1E-12	5.52E-13	106
RH106M	5.49E-11	2.85E-14	0	0	106
RU106	2.33E-06	2.32E-06	1.17E-06	5.87E-07	106
AG107	2.43E-13	2.44E-13	5.17E-13	7.91E-13	107
PD107	2.56E-06	2.56E-06	2.56E-06	2.56E-06	107
AG108	2.07E-17	3.52E-23	3.5E-23	3.48E-23	108
AG108M	1.12E-14	1.12E-14	1.11E-14	1.1E-14	108
CD108	1.28E-12	1.28E-12	1.28E-12	1.28E-12	108
PD108	1.62E-06	1.62E-06	1.62E-06	1.62E-06	108
AG109	8.86E-07	8.88E-07	8.89E-07	8.89E-07	109
AG109M	3.22E-12	9.41E-13	3.02E-22	1.75E-22	109
CD109	5.28E-16	5.27E-16	3.06E-16	1.77E-16	109
AG110	4.16E-13	4.76E-17	1.73E-17	6.28E-18	110
AG110M	3.15E-09	3.14E-09	1.14E-09	4.14E-10	110
CD110	1.43E-07	1.43E-07	1.45E-07	1.45E-07	110
PD110	4.92E-07	4.92E-07	4.92E-07	4.92E-07	110

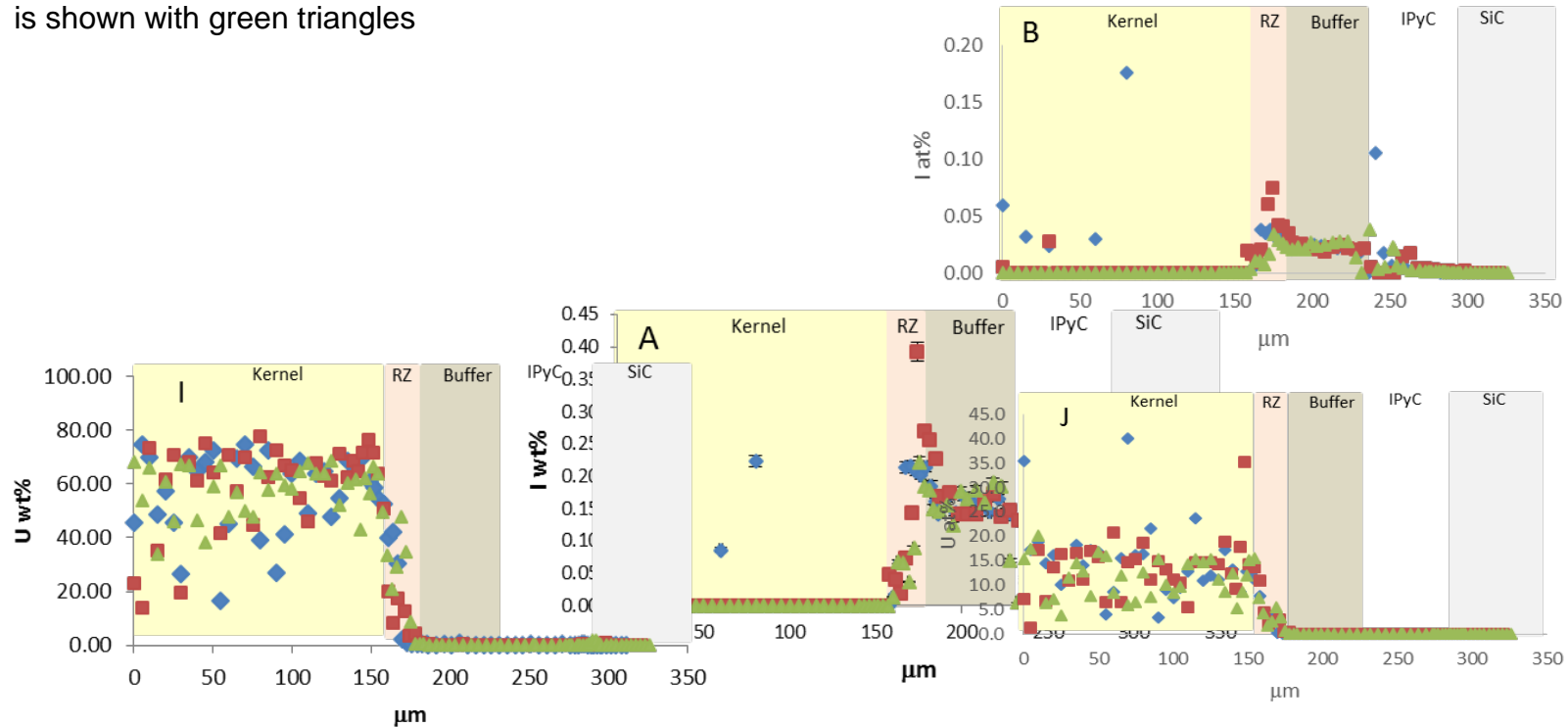
We are currently over 6 years after the end of irradiation

Differences between SEM-EDS and EPMA-WDS

- Energy dispersive spectrometer (EDS) detect and quantify characteristic X-rays generated to determine composition.
- EDS detector simultaneously generate X-rays from all detectable chemical elements. The intensity of the peaks and peak shapes are compared with library spectra of pure specimens to quantify the X-rays and thus produce a chemical composition. The composition can be expressed as atomic percent or weight percent (normalized to 100%). Unknown if there are significant missing analytes, sample porosity, or other issues that cause problems with analysis.
- In contrast, EPMA typically uses a wavelength dispersive spectrometer (WDS) to detect and quantify characteristic X-rays.
 - The WDS detector measures one element at a time, and measures only those elements specified.
 - The intensity of the peaks in the unknown sample is compared to the intensity generated by known standards that were measured prior to measuring the unknown sample.
 - The composition is initially reported as weight percent, which is important because it allows the user to evaluate the quality of the data. For solid, non-porous samples, the weight percent total of all analytes should be close to 100%. When the analyte totals differ significantly from 100 weight percent, it is because an analyte that is present was not measured, the sample is porous or of irregular topography, or because of other analytical issues that require resolution.
- When the weight percent analyte totals are close to 100%, the data can be cast as atomic percent without skewing the data. The reason for this is because the first step to recasting a sample composition from weight percent to atomic percent is to normalize the analyte weight percent total to 100%. If the analyte totals are not close to 100%, the normalization process can skew the data.

EPMA: Atomic vs Weight % reporting

AGR1-433-003 (non-defect side) is shown with blue diamonds, the defect side is shown with red squares and AGR1-433-007 is shown with green triangles



		35v non-buge side atomic %																							
	Tc at%	I at%	Xe at%	Cs at%	Pd at%	Cd at%	Ag at%	U at%	Ba at%	La at%	Ce at%	Pr at%	Nd at%	Sm at%	Eu at%	Sr at%	Ru at%	Mo at%	Zr at%	Tc at%	Cat%	O at%	Si at%	Sr at%	Total
0	0.12	0.06	0.03	0.00	0.32	0.22	0.00	35.4	0.13	0.80	1.74	0.69	2.15	0.35	0.00	0.00	2.38	3.25	2.81	1.18	15.5	30.5	2.22	0.22	100
5	0.03	0.00	0.00	0.00	0.01	0.04	0.00	17.2	0.01	0.32	0.60	0.25	0.95	0.17	0.02	0.01	0.03	0.09	0.07	0.05	34.7	45.5	0.00	0.07	100
10	0.04	0.00	0.00	0.00	0.13	0.04	0.00	19.0	0.01	0.16	0.47	0.16	0.54	0.10	0.01	0.00	0.33	3.27	4.67	0.42	21.5	49.1	0.00	0.05	100
15	0.00	0.03	0.00	0.01	0.03	0.07	0.29	14.4	0.00	0.42	0.77	0.20	0.49	0.05	0.00	0.01	0.00	0.94	1.15	0.36	53.2	27.2	0.26	0.08	100
20	0.00	0.00	0.00	0.00	0.21	0.06	0.01	16.1	0.04	0.02	0.04	0.03	0.09	0.05	0.00	0.00	0.06	0.11	0.10	0.00	18.2	64.8	0.02	0.04	100
25	0.00	0.00	0.01	0.00	0.14	0.03	0.00	10.1	0.03	0.04	0.18	0.10	0.19	0.03	0.00	0.00	1.25	0.66	3.90	0.16	29.9	53.1	0.09	0.06	100
		35v Buge side weight %																							
um	Te wt%	I wt%	Xe wt%	Cs wt%	Pd wt%	Cd wt%	Ag wt%	U wt%	Ba wt%	La wt%	Ce wt%	Pr wt%	Nd wt%	Sm wt%	Eu wt%	Sr wt%	Ru wt%	Mo wt%	Zr wt%	Tc wt%	C wt%	O wt%	Si wt%	Sr wt%	Total
0	0.00	0.01	0.00	0.00	0.01	0.04	0.00	22.9	0.00	0.29	0.64	0.30	1.08	0.25	0.01	0.00	0.03	0.16	0.09	0.04	5.02	12.9	0.07	0.02	43.8
5	0.00	0.00	0.18	0.00	0.26	0.01	0.85	13.9	0.00	0.43	1.21	0.61	2.35	0.46	0.06	0.00	0.20	1.01	2.62	0.14	38.4	19.9	0.24	0.04	82.8
10	0.11	0.00	0.00	0.01	0.04	0.07	0.00	73.2	0.02	0.12	0.30	0.21	0.89	0.17	0.00	0.00	0.42	1.56	0.02	5.97	15.0	0.00	0.07	98.2	
15	0.05	0.00	0.01	0.00	0.14	0.00	0.26	35.2	0.04	0.64	0.99	0.23	1.57	0.30	0.06	0.02	0.62	3.44	3.70	0.41	16.8	8.2	0.08	0.06	72.8
20	0.09	0.00	0.00	0.00	0.04	0.09	0.00	61.8	0.05	0.52	1.20	0.49	1.60	0.28	0.02	0.01	0.08	2.06	0.73	0.34	3.99	19.9	0.00	0.03	93.3
25	0.12	0.00	0.00	0.01	0.00	0.08	0.00	70.8	0.04	0.59	1.03	0.68	2.69	0.53	0.05	0.03	0.30	0.22	0.09	0.10	2.17	20.7	0.00	0.08	100.3